AD-A099 781 NAVAL UNDERWATER SYSTEMS CENTER NEW LONDON CT NEW LO--ETC F/G 13/13
DYNAMICS OF UNDERSEA CABLES.(U)
MAY 81 J M SYCK
UNCLASSIFIED NUSC-TR-6313 NL

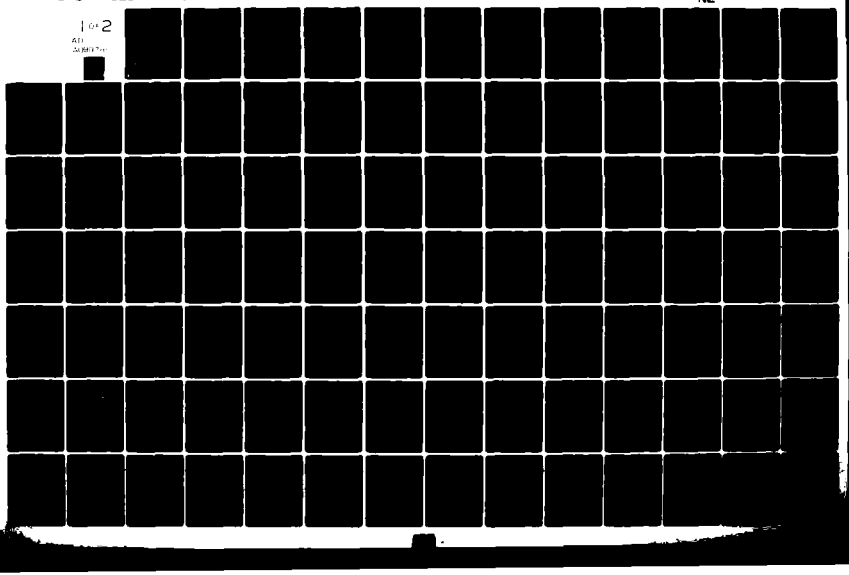

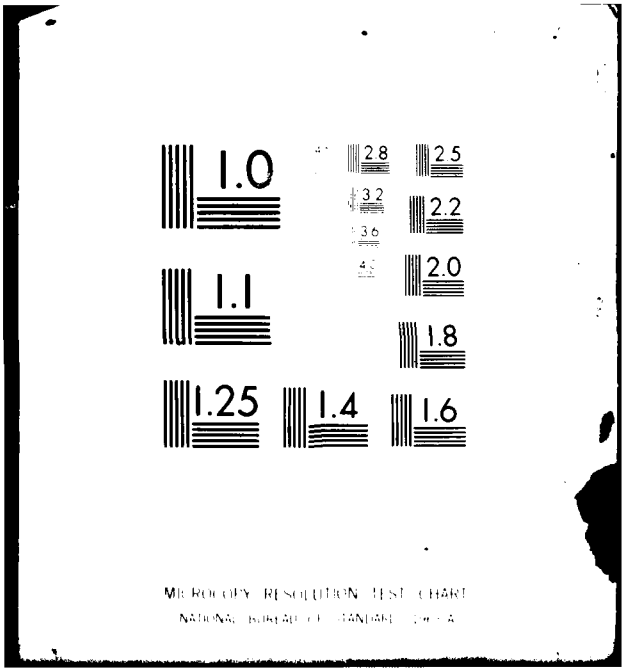
1.0
2.8
2.5
3.2
2.2
3.6
4.5
2.0
1.1
1.8
1.25
1.4
1.6
MICROCOPY RESOLUTION TEST CHART
NATIONAL BUREAU OF STANDARDS 1963-A

NUSC Technical Report 6313
17 May 1981

Dynamics of Undersea Cables

James Marvin Syck
Surface Ship Sonar Department

Naval Underwater Systems Center
Newport, Rhode Island / New London, Connecticut

Preface

This report was prepared initially as a dissertation submitted in partial fulfillment of the requirements for the degree of Doctor of Philosophy, University of Miami, Coral Cables, Florida.

I wish to thank the members of my committee, Profs. H. A. DeFerrari, B. E. Howard, F. P. Tappert, K. D. Leaman, and S. C. Daubin for their encouragement during the course of this study. I also wish to thank my colleagues Gary Griffin and Peter Herstein for their help with a stubborn computer and for always being available for discussion of the problem. Dr. B. E. Howard provided considerable assistance and encouragement during a summer study appointment at the Naval Underwater Systems Center. D. J. Meggitt provided computer output from the DECELI static deflection program implemented at the Navy Civil Engineering Laboratory, Port Hueneme, California. Finally, a word of appreciation for my wife who provided continuous support and encouragement throughout the course of this work.

Reviewed and Approved: 17 May 1981

D. Walters
Head, Surface Ship Sonar Department

The author of this report is located at the New London Laboratory, Naval Underwater Systems Center, New London, Connecticut 06320.

REPORT DOCUMENTATION PAGE		READ INSTRUCTIONS BEFORE COMPLETING FORM
1. REPORT NUMBER TR 6313	2. GOVT ACCESSION NO. AD-A099 782	3. RECIPIENT'S CATALOG NUMBER
4. TITLE (and Subtitle) (4) DYNAMICS OF UNDERSEA CABLES,		5. TYPE OF REPORT & PERIOD COVERED (9) Technical rept.
		6. PERFORMING ORG. REPORT NUMBER
7. AUTHOR(s) (10) James Marvin/Syck	(12) 722	8. CONTRACT OR GRANT NUMBER(s)
9. PERFORMING ORGANIZATION NAME AND ADDRESS Naval Underwater Systems Center New London Laboratory New London, Connecticut 06320		10. PROGRAM ELEMENT, PROJECT, TASK AREA & WORK UNIT NUMBERS A64885
11. CONTROLLING OFFICE NAME AND ADDRESS (11)		12. REPORT DATE 17 May 1981 13. NUMBER OF PAGES 102
14. MONITORING AGENCY NAME & ADDRESS(if different from Controlling Office) (14) NUSC-TR-6313		15. SECURITY CLASS. (of this report) UNCLASSIFIED 15a. DECLASSIFICATION/DOWNGRADING SCHEDULE

16. DISTRIBUTION STATEMENT (of this Report)

Approved for public release; distribution unlimited.

17. DISTRIBUTION STATEMENT (of the abstract entered in Block 20, if different from Report)

18. SUPPLEMENTARY NOTES

19. KEY WORDS (Continue on reverse side if necessary and identify by block number)

Marine cables
Mathematical models
Ocean currents
Dynamic models
Steady State models
Strumming

20. ABSTRACT (Continue on reverse side if necessary and identify by block number)

Mathematical models have been used for some time to predict the deformation of undersea cables due to ocean currents; however, there have been very few measurements made that permit verification of model results against observations of cable deformation. A dynamic model and a static model have been used to make calculations of shape for an experimental acoustic array deployment in the North Atlantic Ocean. The calculations were then compared to careful measurement of the shape of the array, which was a cable 6 km long suspended several kilometers above the sea floor. Both models are in (over)

DD FORM 1 JAN 73 1473 EDITION OF 1 NOV 65 IS OBSOLETE
S/N 0102-014-6601

20. (Cont'd)

qualitative agreement with observation, but they underestimate the magnitude of the maximum deformation by a factor of about 2. This underestimation has been observed before and is commonly attributed to neglect of strumming in the models. Several methods are tried to introduce strumming effects in models, but none are wholly successful. Static models do not fit the experimental data as well as the dynamic model.

TABLE OF CONTENTS

TABLE OF CONTENTS (Cont'd)

LIST OF TABLES

LIST OF ILLUSTRATIONS

LIST OF ILLUSTRATIONS (Cont'd)

DYNAMICS OF UNDERSEA CABLES

1. INTRODUCTION

1.1 Statement of the Problem

There is a plethora of computer models which compute the shape of cables subject to ocean current forcing. In a summary report Albertson[1] listed 44 different models currently in use. There is very little data, however, which can be used to compare the model outputs with experimentally observed cable shapes.

The governing equations which describe the cable response to ocean current forcing are a set of nonlinear partial differential equations. Various investigators have simplified the equations in several ways to facilitate their solution. In the absence of experimental data, however, there is very little basis on which to decide the relative importance of the various simplifications that have been made.

The object of this study is to examine several model types, introduce measured ocean currents, compare the outputs with a set of carefully made measurements of cable shape, draw conclusions concerning the validity of the models in this particular setting, and recommend improvements in the models.

1.2 Background

Over the years there have been numerous studies of the problem of the shape of a cable subjected to various forces. The first analytical work was that of James Bernoulli, who in 1690 studied the equilibrium shape of a uniform chain supported at the ends. This work resulted in

the catenary equations.[2] Since that time the literature has grown, as can be seen in table 1.

Table 1. Number of Citations Listed in Recent Review Papers

Review Paper	Number of Citations	Topic of Review
Davis, Fitzgerald and Neilligan (1963)[3]	101	Deep Sea Moorings
Casarella and Parsons (1970)[4]	81	Cable Motion Under Hydrodynamic Loading
Albertson (1974)[1]	107	Submerged Moorings
King (1980)[5]	68	Vortex Shedding

Given the size of the body of literature on the topic, one would think that the problem would now be solved. This is not the case. The characterization of the drag forces is an active area of research. Also it is not yet possible to solve the complete equations of motion of complex cable structures in a reasonable period of time on existing computers. In order to proceed with the solution to the problem, experimental data must be obtained which can be used to test cable models. The data set would permit testing of drag force models and would allow quantitative assessment of the effects of candidate simplifications of the complete equations of motion which would facilitate implementation of the models on computers. The few measurements made to date do not provide adequate data for comparison of theory with observation. It turns out that it is very difficult to make the required measurements, because what is needed is an accurate physical description of the cable system, currents measured in sufficient detail to define flow variations along the

length of the cable, and measurement of cable position at a sufficient number of points to describe cable shape. Some work has been done; measurements on a laboratory scale have been made,[6,7] and work has also been reported on limited measurements made at sea.[8,9]

A comprehensive review of research investigations on the prediction of motion of cable systems under hydrodynamic forcing was performed by Casarella and Parsons.[4] They trace the development from World War I era attempts to develop analytical models for the two-dimensional, steady-state cable problem, motivated by the requirement for predicting the height of barrage balloons in varying wind conditions. Two-dimensional dynamic models are of more recent origin, coming after World War II. Some of this work was stimulated by the requirement for modeling the two-dimensional dynamic motion of ships during the nuclear testing program in the Pacific. The three-dimensional problem began to be addressed in the 1960's, motivated by the need for models to describe the motion of towed bodies and tow cables, and the need to describe mooring motions for both surface platforms and oceanographic measurement moorings. Particularly important work in this period was that of Wilson[10] and Reid.[11]

The widespread use of large computers for numerical solution of the cable equations led to major steps forward in the 1970's. Bedenbender[12] solved the three-dimensional static configuration problem using a predictor-corrector method, then solving the two point boundary value problem by a shooting technique. DeZoysa [13] improved the method of solution to give convergent solutions in certain problem cases when the initial guess at the solution was poor. Skop and O'Hara[14] and Skop and

Mark[15] developed a three-dimensional cable model for predicting equilibrium configurations of moored cable systems using the method of imaginary reactions.

The three-dimensional dynamic cable problem has been solved by Patton[9] by considering a lumped mass system. In this formulation of the problem the forces that operate over the entire cable are considered to operate at discrete points along the cable. Essentially the model is one in which the array is considered to be a set of discrete masses connected by massless springs. A two-dimensional problem of this type was solved earlier by Paquette and Henderson on an analog computer.[16]

Finite element formulations of the cable dynamics problem have been given by Morgan[17] and Webster.[18]

In addition to the development of increasingly more complex models, simplified models for the purpose of engineering calculations were developed.[19,20] These simplifications provided quick calculations of parameters of importance to the design of certain simple moorings.

1.3 Current Status of the Problem

The cable equations must be solved numerically, because analytic solutions, except in the simplest situations, cannot be obtained. It is possible to obtain solutions using existing numerical models for the equilibrium configuration of complex cable structures such as multilegged moorings. The moorings may incorporate buoys and other discrete discontinuities. Variations in the magnitude and direction of ocean current as a function of position on the structure can be accommodated. Cables with nonuniform material properties and elastic cables can be modeled. In short, static models can provide calculations for almost the whole

range of situations of practical interest. What is not known is how closely the models represent physical systems. There is also some uncertainty about input parameters such as normal and tangential drag coefficients and strumming parameter.

A similar situation exists with respect to dynamic models. The models promise to deliver the answers to almost any practical problem. There is an additional complication, however: The solutions generally require substantially greater amounts of computer time.

> Albertson conducted a survey of existing cable models and concluded, "Precise validation data for the steady-state and dynamic programs are needed to quantify the errors associated with the various techniques and to help select correct hydrodynamic loading criteria and added mass and damping coefficients used in the computer programs."[1]

While some progress has been reported,[8,21] the preceding statement is still generally true. This study will attempt to fill this critical gap by reporting the results of measurements of cable position as a function of time for a large cable system. Ocean currents measured at two locations near the cable are input into several models and the model results are compared to the observed cable shape.

2. CABLE EQUATIONS

2.1 Dynamic Equations

The equations governing the motion of a cable system are derived from Newton's second law:

$$\sum \vec{F} = \vec{ma} \tag{1}$$

where the forces to be considered are gravity, tension, damping, viscous drag and hydrodynamic inertia. Mathematical formulations of these forces are given in Reid.[11] The general formulation of the equations of motion requires consideration of the elastic properties of the cable. In order to do this a Lagrangian coordinate, S_o, is generally employed. S_o is the coordinate on the original unstretched cable and S is the corresponding coordinate on the stretched cable.

Keller[22] showed that Lagrangian coordinates lead to a particularly simple form for the equations of motion for a string. In this formulation it was not necessary to make the assumption that the motions were small. Keller, however, went on to assume a particular form of the stress/strain relationship which does not generally hold.

Cristescu,[23,24] using Lagrangian coordinates, wrote the equations of motion for an elastic string in the following form:

$$\frac{\partial}{\partial S_o}\left(\frac{T}{1+\epsilon}\frac{\partial x}{\partial S_o}\right) - \rho_o \frac{\partial^2 x}{\partial t^2} + (1+\epsilon) X = 0 \tag{2}$$

$$\frac{\partial}{\partial S_o}\left(\frac{T}{1+\varepsilon}\frac{\partial y}{\partial S_o}\right) - \rho_o \frac{\partial^2 y}{\partial t^2} + (1+\varepsilon)\,Y = 0 \qquad (3)$$

$$\frac{\partial}{\partial S_o}\left(\frac{T}{1+\varepsilon}\frac{\partial z}{\partial S_o}\right) - \rho_o \frac{\partial^2 z}{\partial t^2} + (1+\varepsilon)\,Z = 0 \qquad (4)$$

where S_o is the Lagrangian coordinate along the unstretched cable; t is time; T is tensile stress: ρ_o mass per unit length of cable, it is related to the mass per unit length of the stretched cable by $\rho_o = (1+\varepsilon)\rho$; X, Y, Z, the components of external forces acting on the cable; ε is strain:

$$\varepsilon = \frac{dS - dS_o}{dS_o} = \sqrt{\left(\frac{\partial x}{\partial S_o}\right)^2 + \left(\frac{\partial y}{\partial S_o}\right)^2 + \left(\frac{\partial z}{\partial S_o}\right)^2} - 1 \qquad (5)$$

where S is the stretched curvilinear coordinate. A very readable derivation of the equations of motion in this form is available in Berteaux.[20] A constitutive law relating stress and strain is also required. Cristescu used the relation $T = E\varepsilon$ in his numerical examples, where T is stress and E is the dynamic elastic modulus. It is assumed that the cable is perfectly flexible; that is, tension is always in the direction of the tangent to the cable. The effects of drag, hydrodynamic mass, and other outside forces are lumped in the force components X, Y, and Z.

The equations are hyperbolic partial differential equations. Cristescu solved them using the method of characteristics. He identified two characteristic lines, the first for transverse waves

$$C_I = \pm\sqrt{\frac{T}{\rho_o(1+\varepsilon)}} \qquad (6)$$

the second for longitudinal waves

$$C_{II} = \pm\sqrt{\frac{1}{\rho_o}\frac{dT}{d\varepsilon}} \quad . \tag{7}$$

In general, both types of waves are always present. The equations may now be integrated using standard numerical techniques such as those given in Forsythe and Wasow.[25] Detailed derivation of the characteristic forms of the equation of motion are given in Reid.[11]

Cristescu performed a direct numerical integration of the equations of motion using the methods outlined above. However, the cases considered were particularly simple. They dealt with a homogeneous string with no external force components ($X = Y = Z = 0$). Unfortunately, even on fast computers direct integration schemes are executed very slowly.[26] This is because the wave speeds, particularly for longitudinal waves, are high (3300 m/sec for steel cable).[11] Consequently, the step size (length and time) must be small. One method to reduce the execution time is to use a lumped-mass model.[9] In this type of model all of the essential dynamics are considered to be acting at a small number of discrete points. The lumped mass points are then considered to be connected by massless springs. The computer running time for this type of model is substantially reduced, but still large. On a Univac 1108 computation time is about equal to simulation time. The price one pays for this reduction is that the small scale behavior is lost. For most undersea cable problems this is not a serious deficiency.

Patton[9] rewrote the Cristescu equations for a lumped mass model, assuming that a uniform cable of unstretched length L can be broken up

into n equal length segments. The length of a segment is $\Delta L = L/n$. All the forces acting on a segment are assumed to be concentrated at the midpoint of the segment:

$$\rho_o \Delta L \frac{d^2 x_n}{dt^2} = X_n \Delta L(1+\epsilon) + T_{x,n} - T_{x,n-1} \tag{8}$$

$$\rho_o \Delta L \frac{d^2 y_n}{dt^2} = Y_n \Delta L(1+\epsilon) + T_{y,n} - T_{y,n-1} \tag{9}$$

$$\rho_o \Delta L \frac{d^2 z_n}{dt^2} = Z_n \Delta L(1+\epsilon) + T_{z,n} - T_{z,n-1} \tag{10}$$

where the symbols have the same meaning as before; the subscript n refers to the n^{th} segment; and the subscripts x,y,z refer to the component of tension resolved along the corresponding coordinate axis. An effective spring constant is given by

$$K = \frac{\pi d^2 E}{4\Delta L} \tag{11}$$

where the symbols have the same meaning as before. The tension in the n^{th} segment is then calculated from

$$T_n = K\left(\sqrt{(x_{n+1} - x_n)^2 + (y_{n+1} - y_n)^2 + (z_{n+1} - z_n)^2} - \Delta L\right) \tag{12}$$

The quantity under the radical is the stretched length of the n^{th} segment.

The forces X_n, Y_n, Z_n are the sums of the force components in the x, y, z directions. They include the forces of hydrodynamic inertia,

viscous drag, gravity and damping. They are calculated according to the formulae presented in sections 2.3 and 2.5.

A more complete theory would allow for variations in the material properties such as

1. creep under constant load
2. time dependent relaxation of elastic strain under no load
3. hysteresis under cyclic loading
4. hydrostatic pressure effects on material properties
5. cable bending stiffness.

These properties are generally ignored in cable behavior models either because the effects are expected to be small or because the data base on material properties is too small to justify inclusion.[11]

In any specific problem one or more of the properties in the preceding list may have to be included. If that turns out to be the case then additional experimental data on the material properties will have to be determined. In the experimental situation to be discussed later in this paper only hydrostatic pressure effects turn out to be important. The tensions are such a small percentage of the ultimate strength that the behavior is essentially that of a linear spring, the cable is so long that it can safely be considered to be limp, and the values of buoyancy at high values of pressure are measured experimentally.

2.2 Steady State Equations

The differential equations governing the equilibrium configuration of an undersea cable have been derived by Patton,[9] Bedenbender,[12] Daubin,[27] DeZoysa,[13] Berteaux[20] and others. Aside from differences in notation and convention in the measurement of angles all of the resulting

systems of equations are identical. The notation adopted in this section is that of DeZoysa.[13] The assumptions inherent in the derivation are as follows:

1. The forces are time independent.
2. Cable ends are under constant tension.
3. Cable is completely flexible and inextensible.

The local coordinate system for an element of cable length ds is shown in figure 1. In this figure, i_s is a unit vector tangent to the cable, i_ϕ is a unit vector normal to the cable and in the vertical plane, i_θ is normal to i_s and i_ϕ and in the horizontal plane.

The equations are derived by resolving the components of force along the i_s, i_ϕ, i_θ directions and then neglecting terms which are products of differential quantities. The resulting set of equations is

$$\frac{dT}{ds_o} = w \sin \phi - R_s \tag{13}$$

$$T \cos \phi \frac{d\theta}{ds_o} = - R_\theta \tag{14}$$

$$T \frac{d\phi}{ds_o} = w \cos \phi - R_\phi \tag{15}$$

$$\frac{dx}{ds_o} = \cos \theta \cos \phi \tag{16}$$

$$\frac{dy}{ds_o} = \sin \theta \cos \phi \tag{17}$$

$$\frac{dz}{ds_o} = \sin \phi \tag{18}$$

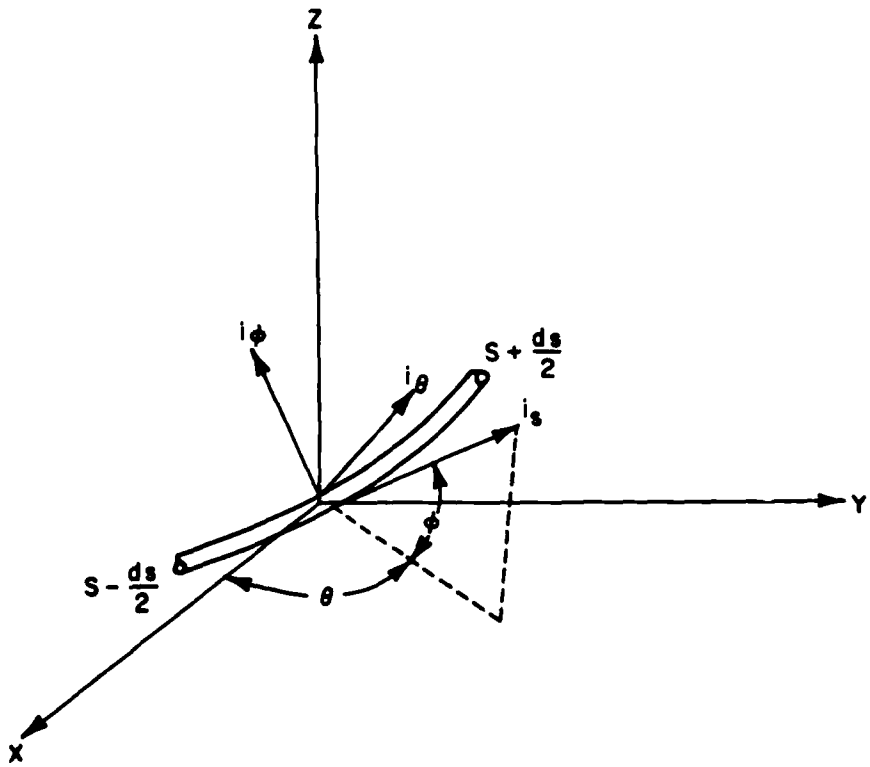

Figure 1. Local Coordinate System for an Element of Cable

where

x,y,z are Cartesian coordinates,

T is tension in the cable,

s_o is arc length along the cable,

w is weight per unit length of cable in the fluid medium,

θ is the angle between the positive x axis and the plane containing the element ds,

ϕ is the angle between ds and the x-z plane,

R_s, R_θ, R_ϕ are hydrodynamic forces along cable coordinates.

Equations 13 through 18 constitute the steady state cable equations. These are six equations in which the independent variable is s_o, and the dependent variables are x,y,z,T,ϕ,θ. The equations can be numerically integrated and the problem then becomes one of solving a two-point boundary value problem. A "shooting method" has been employed by Bedenbender[12] and DeZoysa.[13] The integration method used was a fourth order Runge-Kutta.

It is also possible to include the elastic properties of the cable. In this case the equations are written in terms of the stretched length, ds:

$$ds = ds_o(1+\varepsilon) \tag{19}$$

where ds_o refers to the unstretched length and ε is the strain. Patton[9] and Radochia[28] provide computer programs for integrating the equations for the elastic cable case.

Generally, however, the equations are not solved directly. The problem is that the equations are nonlinear. The method of solution

employed in each of the steady state models considered in this study depends on a variant of the method of imaginary reactions. This is a method borrowed from structural analysis.[14,15,29] In this method positions of points on the array are found by the rules of statics without recourse to solving the nonlinear force balance equations of the system. A lumped parameter representation of the forces involved is used. One calculates the sum of the forces and an assumed or imaginary reaction at an anchor. An equilibrium configuration is calculated from the balance of forces which will be inconsistent with some geometric constraint such as the known anchor separation in a two anchor system. The vector difference between the solution from the calculated position and the known position is used to correct the imaginary reaction, and the process is repeated until the error is less than a specified amount. A straightforward exposition on this topic can be found in Berteaux.[20]

2.3 Drag Forces

There is considerable uncertainty as to the form of the forcing functions that drive the system. Prior to the mid 1950's most cable analyses used a form of the normal component of drag force given by

$$D = C_D \frac{1}{2} \rho d V^2 \sin^2 \phi \tag{20}$$

where D is drag force per unit length of cable, C_D is a drag coefficient, ρ is the mass density of the fluid, V is the speed of the current, d is the diameter of the cable, and ϕ is the angle between the tangent to the cable and the current vector. Tangential drag was considered small and nearly constant.[4]

More recently, however, this simple drag model has been found inadequate, particularly with respect to tangential drag. Even though the values of the tangential drag force are two orders of magnitude smaller than the normal drag force, in many cable problems, it can be important.[10] A commonly used force model was formulated by Eames.[30] The normal component of force per unit length of cable is given by,

$$F_n = \frac{\rho d C_D}{2} V^2 \{(1-\mu) \sin \phi |\sin \phi| + \mu \sin \phi\} \quad . \tag{21}$$

The tangential component of force per unit length of cable is given by

$$F_t = \frac{\rho d C_D}{2} V^2 \{\mu \cos \phi + \nu \cos \phi |\sin \phi|\} \tag{22}$$

where

F_n is normal component of force,

F_t is tangential component of force,

ρ is density of fluid,

C_D is drag coefficient,

ϕ is angle between cable tangent and flow direction,

d is diameter of cable,

μ is friction coefficient
ν is form drag coefficient
} both range from 0.025 to 0.05.

Wilson[10] summarized a large number of drag coefficient measurements as a function of Reynolds number. From his data we get the commonly used values of 0.9 to 1.2 for smooth cables and 1.4 for rough cables in the Reynolds number range commonly found in the sea. There is considerable

scatter in the data, however, and any particular cable is likely to vary from the norm. For example, Kretschmer, Edgerton, and Albertson[31] performed wind tunnel tests on a jacketed cable 1.8 cm (0.705 in.) in diameter and obtained drag coefficient values of 1.55 for the Reynolds number range commonly experienced in the ocean. This is somewhat higher than the results for smooth rigid cylinders.

The Reynolds number of the flow is given by

$$R_e = \frac{Vd}{\nu} = \frac{\rho V d}{\mu} \tag{23}$$

where

R_e is Reynolds number

ν is kinematic viscosity

μ is dynamic viscosity

d is diameter of the cable

V is velocity of flow

ρ is seawater density.

Typical values for the parameters applicable to the experimental data that will be presented later are: μ at 4°C = 0.016 gm/cm sec,[32] d = 4 cm, V = 2 to 10 cm/sec, and ρ = 1.025 gm/cm^3. Substituting these values in equation (23) gives a Reynolds number range of $0.5 \times 10^3 < R_e < 2.6 \times 10^3$.

The drag force equation used in the Griffin model and the Patton model was that given by equation (20) with the value of C_D calculated as follows for the normal component of drag force:

$$C_D = 1.2\, e^{-\left[\frac{R_e - 200}{8000}\right]} \qquad 200 < R_e < 25{,}000 \tag{24}$$

$$C_D = 0.9\, e^{-\left[\frac{R_e - 2500}{43{,}000}\right]} \qquad 2500 < R_e < 15{,}000 \qquad (25)$$

$$C_D = 1.2 \qquad 15{,}000 < R_e < 200{,}000 \qquad (26)$$

The tangential component of drag was calculated from

$$F_T = \frac{1}{2} \rho\, C_{DT}\, \pi d\, V^2 \cos\phi |\cos\phi| \,. \qquad (27)$$

The expression for the tangential drag coefficient used is based on a study by Wilcox:[33]

$$C_{DT} = 0.8\, (R_{eT})^{-0.77} \qquad 1 < R_{eT} < 10^2 \qquad (28)$$

$$C_{DT} = 0.0635\, (R_{eT})^{-0.22} \qquad 10^2 < R_{eT} < 10^6 \qquad (29)$$

where R_{eT} is the Reynolds number calculated for the tangential component of the flow velocity.

2.4 Strum Amplified Drag Coefficient

There is a further complication to the drag coefficient issue. It is well known that cables in a moving fluid will experience flow induced strumming vibrations.[21] If the strumming frequency approaches the natural frequency of the cable then resonance can occur. The result of this is a greatly increased drag. This idea is used to explain why the observed cable displacements are often much larger than the models predict. Skop and Rosenthal[34] have introduced a strum amplified drag coefficient in the DESADE static model to bring the calculated cable

displacements into better agreement with observations. They give a formula for the strum amplified drag coefficient, C_{DA}, for horizontal cables:

$$\frac{C_{DA}}{C_{DO}} = 1 + \frac{1.69\ R_n^{1.09}}{(\sqrt{R_n} + 4.61)^{2.16}} \tag{30}$$

where C_{DO} is the drag coefficient for a nonstrumming cylinder and R_n is the Reynolds number for the flow based on the component of current normal to the cable axis;

$$R_n = \frac{V_n\ d}{\nu} \tag{31}$$

where V_n is the normal component of flow and ν is the kinematic viscosity of the fluid.

The strumming frequency is determined by

$$f = \frac{S_n\ V_n}{d} \tag{32}$$

where S_n is the Strouhal number, V_n is the velocity component of the current normal to the cable, and d is the cable diameter. For Reynolds numbers between 10^3 and 10^4 the Strouhal number is nearly constant ~0.21.[35]

The data base on which to decide a priori whether a cable will strum or not is very skimpy. Kennedy and Vandiver[36] summarize the results of four experiments which attempted to measure strumming effects. All of

the experiments suffer from one defect or another, but they were able to draw the following conclusions;

1. Excitation process seems to be a narrowband random process centered around the Strouhal frequency.
2. Many modes of cable oscillation are excited - as many as 50 or 100.
3. Resonant lock-on of cable natural frequency with vortex shedding frequency was observed only rarely.
4. There appears to be a self limiting mechanism for the amplitude response which does not seem to be affected by cable length, virtual mass, damping, number of modes excited, or flow speed.
5. The amplitude of the nonresonant response was about one quarter of a cable diameter.

The literature on vortex induced oscillations is large and there are two excellent review articles by King[5] and Sarpkaya.[37] There is a great deal of controversy in the field and different arguments can be brought to bear to explain the results quoted above. Aside from the work of Skop and Rosenthal[34] (it will be shown later that equation (30) leads to unrealistically high values of the drag coefficient when applied to the experimental data) there is little help for the modeler who is interested in modeling the large scale behavior of cable systems.

The simplest way to account for strumming phenomena is to adjust the drag coefficient, or equivalently, increase the effective cable diameter in the drag force equations. Dale and McCandless suggest a drag coefficient increase of 38 percent based on experimental data with short cables in a tow tank.[38] Conclusion 5 in the preceding list taken

from Kennedy and Vandiver[36] suggests that an increase of effective cable diameter of 25 percent would be appropriate. In the results that follow several drag coefficients will be employed as will an increased effective cable diameter.

2.5 Added Mass

If a cable immersed in a fluid is accelerated, the force required is larger than the force to more just the cable. This is because a part of the fluid must also be moved around the cable. An expression for the force per unit length of cable is

$$F_a = (m + m_a) \frac{dv}{dt} \tag{33}$$

where m_a is the added mass. The quantity $(m + m_a)$ is referred to as the virtual mass. The added mass per unit length of cable can be calculated from

$$m_a = C_m \rho \pi \frac{d^2}{4} \tag{34}$$

where C_m is the added mass coefficient, ρ is the density of the fluid, and d is the cable diameter. C_m can be calculated from potential theory for nonrotating flow of ideal fluids.[39] The value of C_m calculated for a sphere is 0.5 and for a cylinder is 1.0. Patton[40] calculated added mass coefficients for a variety of shapes.

In practical problems, however, we are likely to violate the assumptions under which C_m is calculated. For these problems the added mass should be measured experimentally. Ramberg and Griffin[41] provide a method for measurement of virtual mass by measuring the ratio of

resonant frequency in air to resonant frequency in water. Virtual mass in water is then calculated from

$$M_{water} = \left(\frac{f_a}{f_w}\right)^2 M_{air} \tag{35}$$

where f_a is resonant frequency in air and f_w is resonant frequency in water. Pattison, Rispin, and Tsai[42] provide a collection of measured values of virtual mass.

There is some evidence that there is a frequency dependence to the added mass. Patton,[9] citing experimental results of Miller[43] and Miller and Hagist,[44] used the following expression:

$$m_a = \left(1.0 - 1.62 \times 10^{-6} \frac{\omega d^2}{\nu}\right) \frac{d^2 \pi \rho}{4} \tag{36}$$

where ω is the frequency, d is the cable diameter, and ν is the kinematic viscosity. It is seen that the quantity outside the parentheses is just the added mass of a circular cylinder of unit length. There is also evidence in experimental results reported by Ramberg and Griffin[45] that there is no frequency dependence to added mass. The issue is presently unresolved. This study will use the Patton expression. The questions that need to be addressed in order to resolve this issue are discussed by Sarpkaya.[37]

3. DESCRIPTION OF EXPERIMENT

3.1 OMAT Background

The data reported in this study were obtained as a subset of measurements from a larger experiment. The overall experiment, the Ocean Measurements and Array Technology (OMAT) program, was directed toward system-oriented measurements relative to large aperture acoustic systems. Thus the primary objective of the program was to provide a highly flexible, large aperture acoustic array that could be deployed, recovered, and reconfigured together with associated processing and real-time analysis equipment so that a variety of array/system concepts could be tested using essentially the same hardware. The system was deployed three times in a series of experiments at sea that were conducted during the summers of 1977, 1978, and 1979. The portion of the overall experiment that will be discussed here is the study of the motion of the array cable in the ocean currents.

The general configuration of the experiment is shown in figure 2. The water depth was 5.5 km. The horizontal span was 6 km long and buoyed to a nominal height above the sea floor of 2.7 km. Within a few hours of the beginning of the experiment, an electrical failure developed in approximately the last one third of the cable so that the only useable data were from the eight position sensors closest to the umbilical. The physical description of the cable system is given in table 2.

The measurement site was in the southern Sohm abyssal plain region near 32° N 57° W. The site was chosen initially because it was believed to be quite flat bathymetrically and in an oceanographically quiet

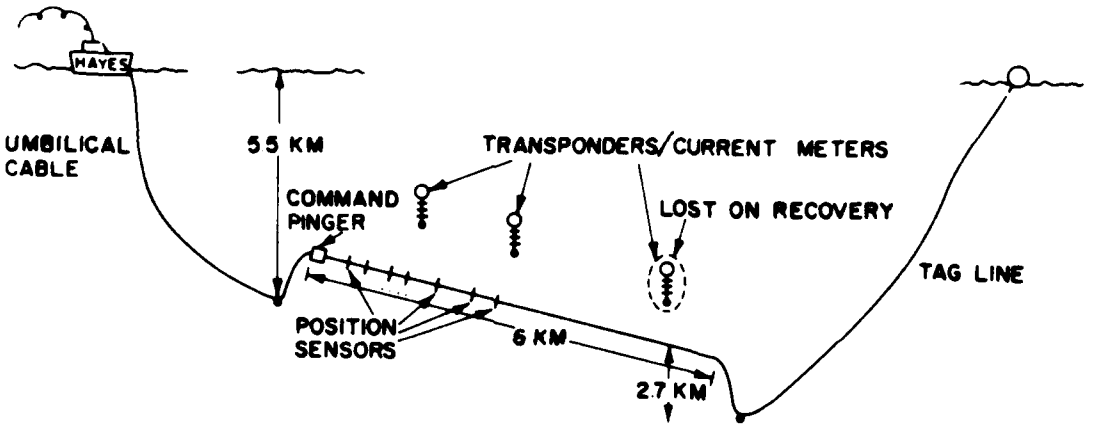

Figure 2. Experiment Configuration

portion of the North Atlantic basin. A bathymetric survey was conducted in the area and a number of small hills were seen to poke out above the generally flat surroundings. Figure 3 shows the results of the site survey and the locations of the anchors and the current meter arrays.

Table 2. Physical Characteristics of the OMAT Cable System

Cable Component	Diameter	Length	Buoyancy in Sea Water	Spring Constant
Umbilical	4.953 cm	9146 m	-2.115 N/m	1.0196×10^7 N/m
Active Riser	5.874 cm	3088 m	4.377 N/m	2.5106×10^6 N/m
Horizontal Span	5.239 cm	5985 m	0.3647 N/m	2.5106×10^6 N/m
Inactive Riser	8.6 cm	3088 m	0.4377 N/m	2.3342×10^6 N/m
Tag Line	4.128 cm	9146 m	0.0 N/m	5.7125×10^6 N/m

A profile measurement was made of temperature, salinity, and sound speed as a function of depth. Density was calculated from the profile measurements and from these data the Brunt-Väisälä frequency was calculated. The profiles of salinity, temperature, sound speed and Brunt-Väisälä frequency are given in figure 4.

3.2 Cable Shape Measurements

The shape of the cable was measured acoustically. The cable shape measurement system consisted of a pinger on the cable, 13 position sensors spaced along the cable, and three transponders located broadside to the cable. Figure 5 shows the arrangement of the components of the cable shape measurement system.

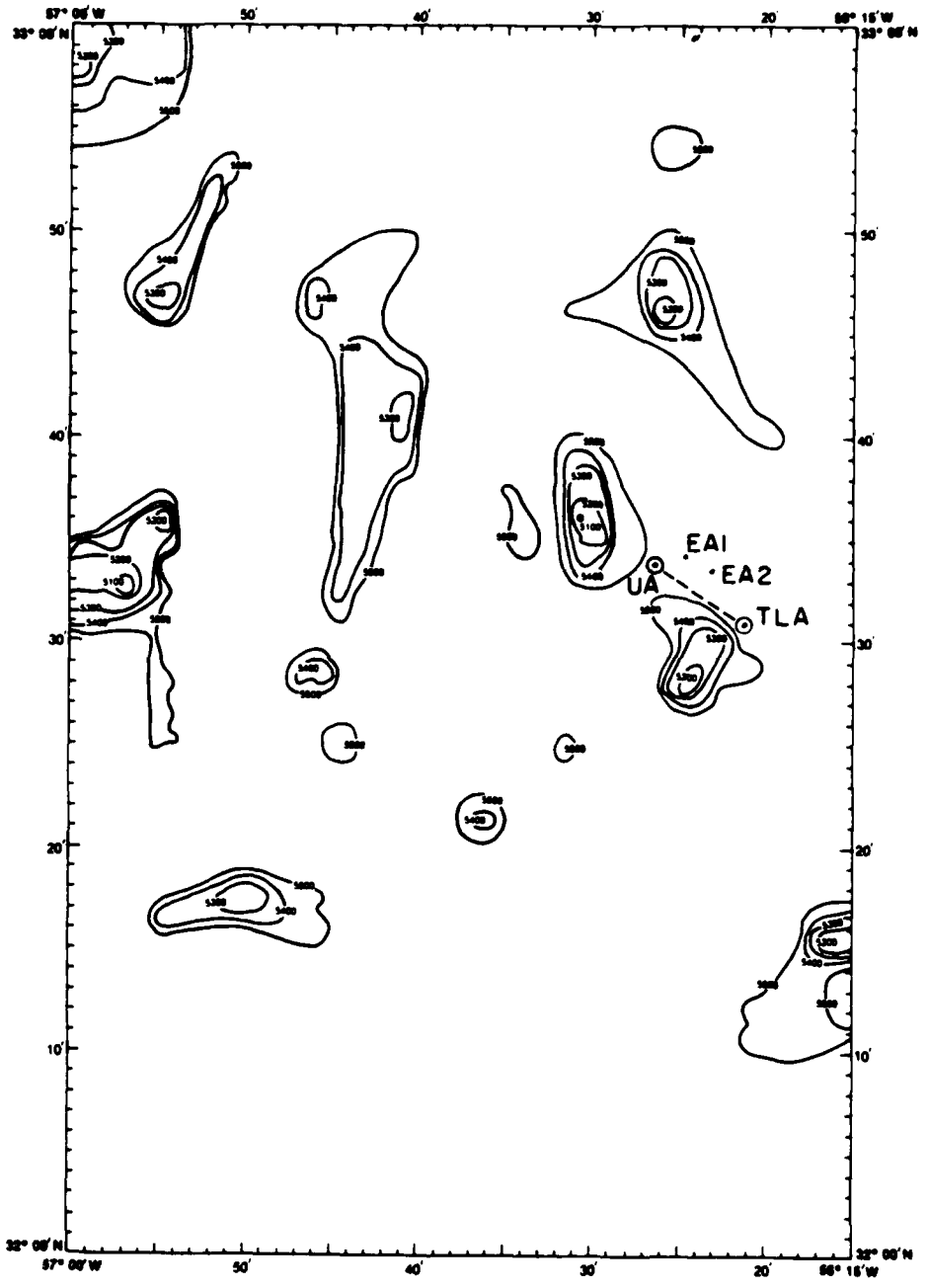

Figure 3. Bathymetry of the Site

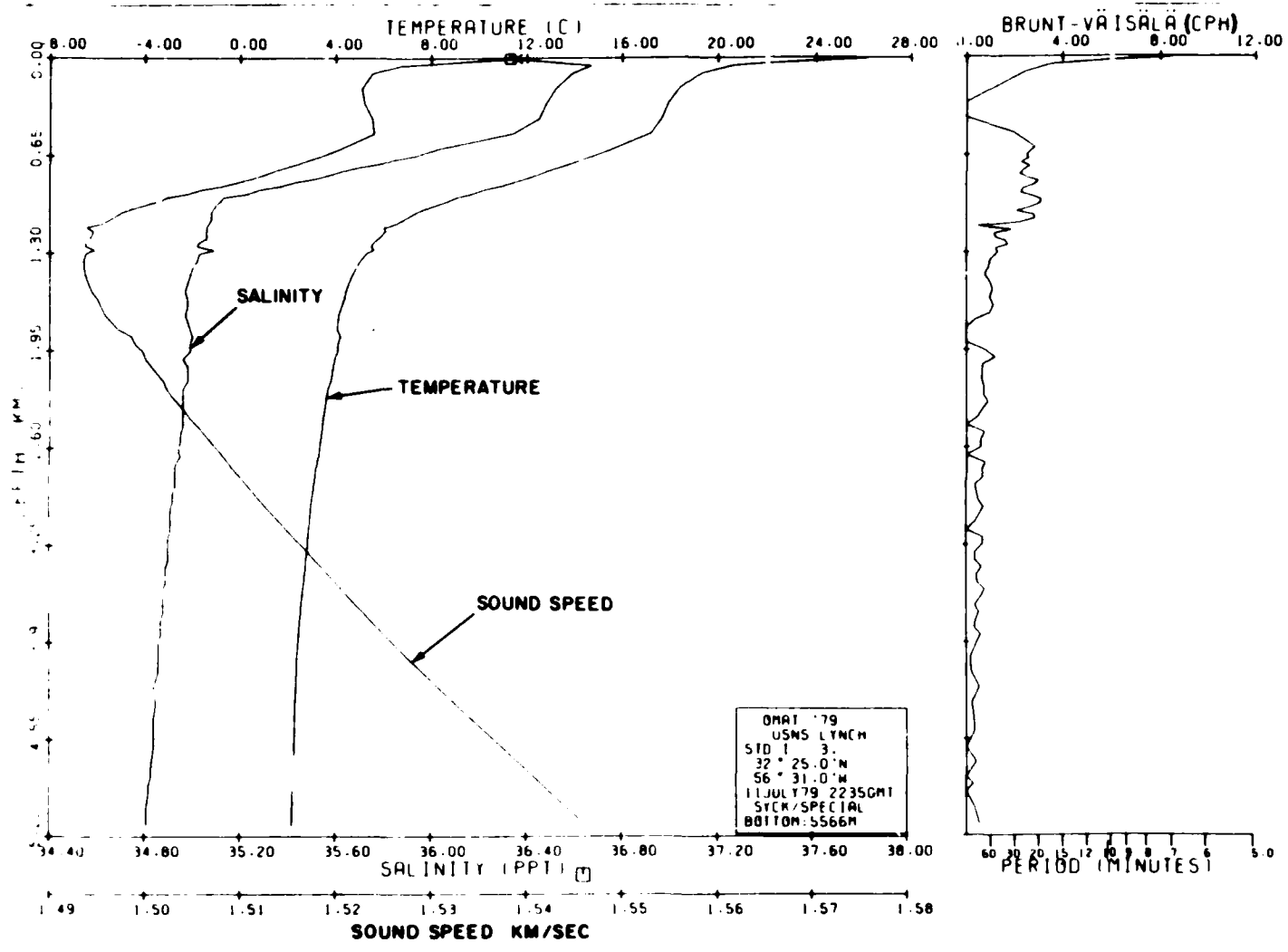

Figure 4. Salinity, Temperature, Sound Speed, and Brunt-Väisälä Frequency at the Site

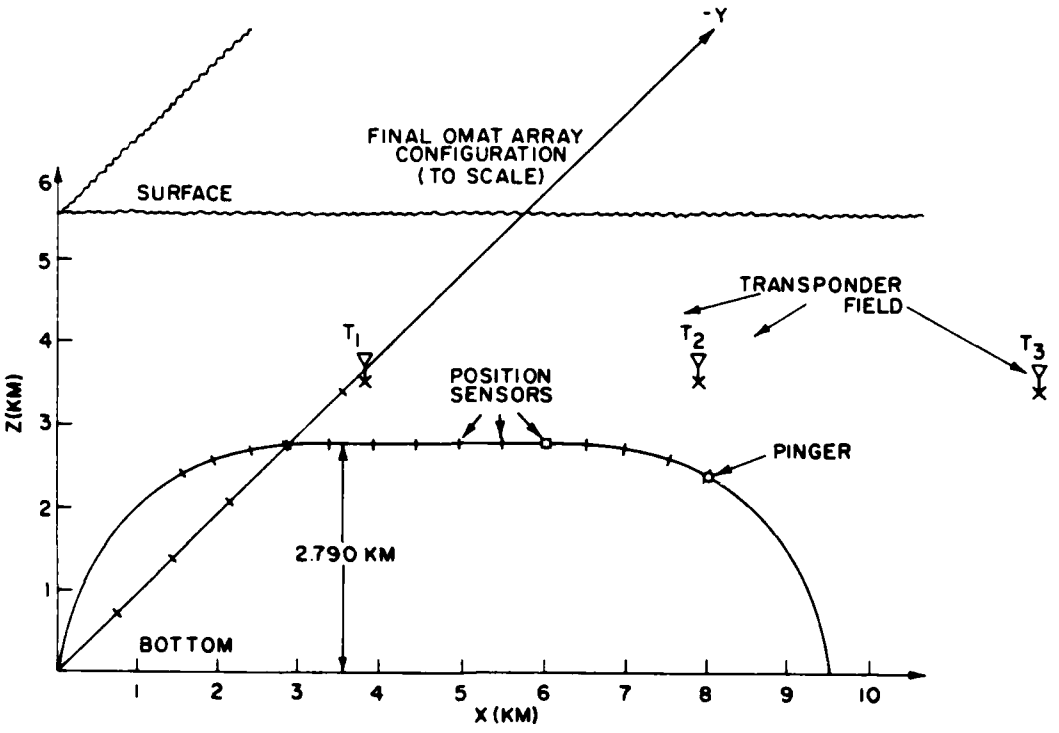

Figure 5. Configuration of Acoustic Cable Shape Measurement System

Table 3 lists the locations of the position sensors relative to the end of the cable.

Table 3. Location of Position Sensors on the Cable

Sensor Number	Distance from End (m)	Remarks
1	24.06	
2	1082.75	
3	1428.25	
4	1913.75	
5	2035.75	
6	2593.25	
7	2930.25	
8	3052.75	
9	3389.75	
10	3943.25	
11	4069.25	
12	4900.25	
13	5958.36	colocated with command pinger, tensiometer and pressure sensor.

The method of cable shape measurement was developed by Callahan.[46] Since his report is unpublished, the features of the technique required to understand the data are summarized here.

The measurement process was initiated on board ship by sending a signal that caused the pinger on the cable to transmit an 11 kHz pulse. This pulse was received at each of three transponders located off to the

side of the cable. The transponders then responded by sending a 9.5, 10.0, or 10.5 kHz pulse, depending on whether the responding transponder was T_1, T_2, or T_3. A signal sequence was then received at each of the position sensors on the cable. All of the received signals were sent via an umbilical cable to a ship nearby where they were stored in a time of arrival matrix for subsequent processing. All of the times stored were relative to the initiating signal sent from the ship.

Acoustic travel time was then converted to slant range using sound speed data measured just prior to the start of the experiment. The sound velocity profile was approximated as piecewise linear. The velocity in layer n is given by

$$v(z) = a_n + b_n(z - z_n) \qquad z_n < z < z_{n+1} \quad . \tag{37}$$

The time for a vertically propagating ray to travel from depth d_1 to d_2 is

$$T(d_1,d_2) = \left| \int_{d_1}^{d_2} \frac{dz}{v(z)} \right| \quad . \tag{38}$$

The average sound speed between depth d_1 and d_2 then is

$$\bar{v}_d(d_1,d_2) = \frac{|d_1 - d_2|}{T(d_1,d_2)} \tag{39}$$

for direct path transmission and

$$\bar{v}_s(d_1,d_2) = \frac{|d_1 + d_2|}{T(0,d_1) + T(d_2,0)} \tag{40}$$

for surface reflected paths. Slant range is then calculated by multiplying the average sound speed for the appropriate path by the observed acoustic travel time. This development assumes straight line ray paths; the error caused by this assumption will be discussed in section 4.2. The pinger depth was determined for each ping by measuring the round trip travel time for the surface reflected ray and converting to depth. The depth of each position sensor R was then calculated for each ping from the known pinger depth T, the direct path length D, and the bounce path length S, according to the relation

$$R = (S^2 - D^2)/4T \quad . \tag{41}$$

The geometry for depth determination is shown in figure 6. Equation (41) is derived using figure 6 by application of the law of cosines:

$$D^2 = a^2 + b^2 - 2ab \cos \theta \quad . \tag{42}$$

Then, drawing the bisector of θ gives

$$\cos \frac{\theta}{2} = \frac{R}{a} \quad . \tag{43}$$

The half angle formula gives

$$\frac{1 + \cos \theta}{2} = \frac{R^2}{a^2} \quad . \tag{44}$$

Solve for cos θ and substitute in equation (42). From the properties of similar triangles

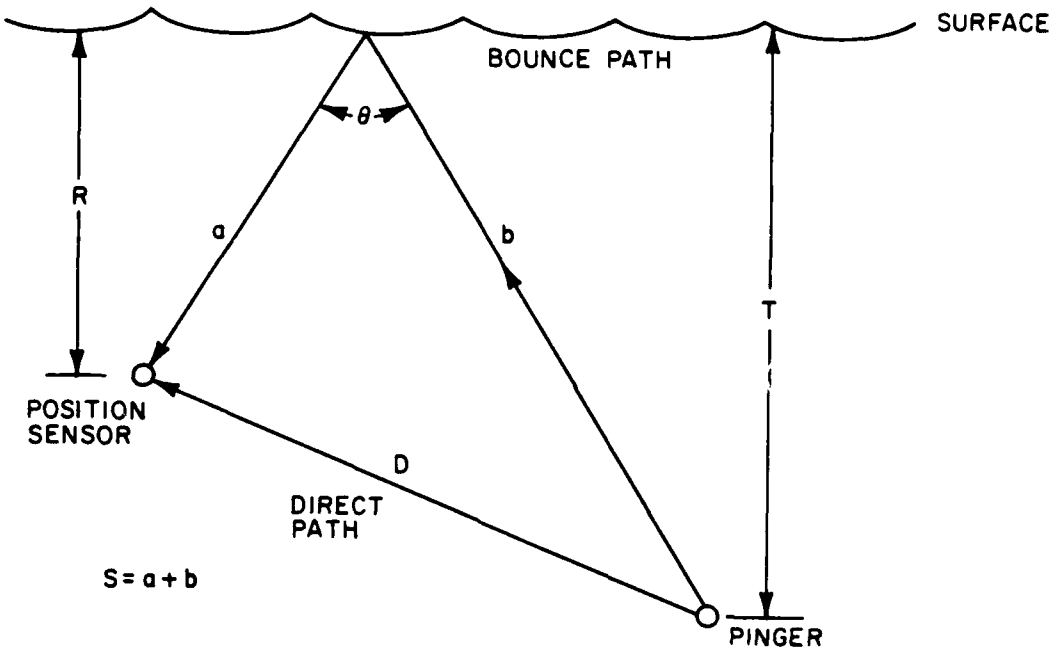

Figure 6. Depth Determination Geometry

$$\frac{b}{a} = \frac{T}{R} . \qquad (45)$$

Making this final substitution and rearranging gives equation (41).

With the depths of all the elements established, it was then possible to project the geometry onto the horizontal plane and calculate the remaining coordinates of each of the sensors. Subsequent calculation would have been straightforward if the transponder positions were known exactly; however, a survey of the transponders conducted from a surface ship shortly after they were installed was not sufficiently accurate. Table 4 provides a comparison of the transponder coordinates determined by survey and a more accurate determination done later by averaging over many sets of cable shape determinations with unknown transponder locations.

Table 4. Transponder Coordinates (km)

	T_1 (x_1,y_1,z_1)	T_2 (x_2,y_2,z_2)	T_3 (x_3,y_3,z_3)
Survey	0.800,-5.355, 0.082	3.365,-5.881, 0.082	8.200,-5.300, 0.082
Post Operation Calculations	0.264,-5.354, 0.082	4.080,-5.863, 0.082	8.522,-5.319, 0.082

The position of each position sensor was found in a coordinate system that had its origin at a transponder and its y axis passing directly below the pinger, as shown in figure 7. The result of this step was

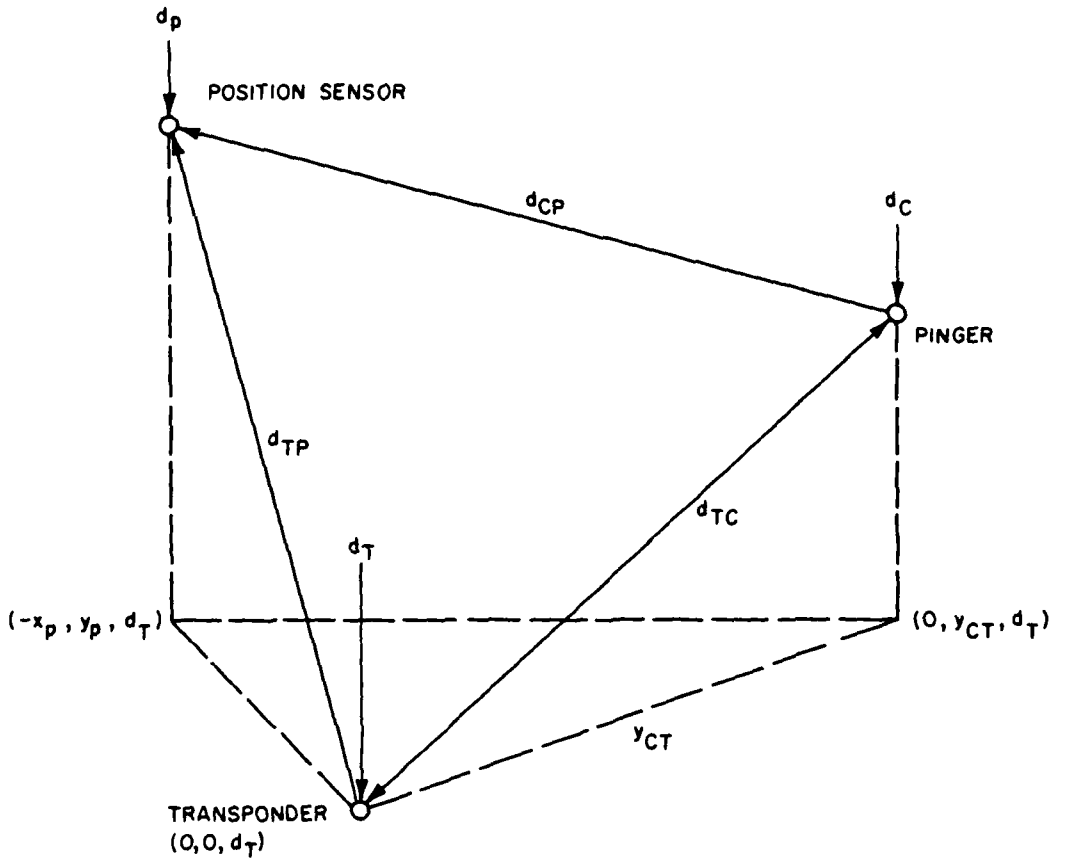

Figure 7. Geometry for Determination of Position Sensor Location in a Transponder Coordinate System

location of all the position sensors in each of three coordinate systems which differ in both origin and orientation, as can be seen in figure 8. The coordinate systems were then rotated and translated by an amount such that the resulting position sensor locations most nearly agreed in a least square error sense.

At this point, what we have is a self-consistent estimate of the position sensor locations, but what we really want is to determine the position sensor locations in a system relative to the two array cable anchors. In order to do this a further fit of the transponder positions was made to the positions obtained from the survey, as this is the only connection between the transponder positions and the array cable anchor positions.

Then, one last rotation and translation is performed to get the final position in the anchor coordinate system.

3.3 Current Meter Measurements

Ocean current data were obtained from two vertical current meter arrays. The two arrays were separated horizontally by 4 km. The location of the measurements was the southern Sohm Abyssal Plain. The array positions relative to the local bathymetry are shown in figure 3. The two arrays were identical. Each array consisted of three Aanderaa RCM 5 current meters. The configuration of the current meter arrays is shown in figure 9. The current meters were epoxy-coated to avoid the compass problem that the older nickel-coated Aanderaa instruments experienced when subjected to high pressure.[47] The instrument heights off the bottom were 646 m, 921 m, and 1530 m. The arrays were designated EA 1 and EA 2 and individual meters on an array were indicated by the suffix

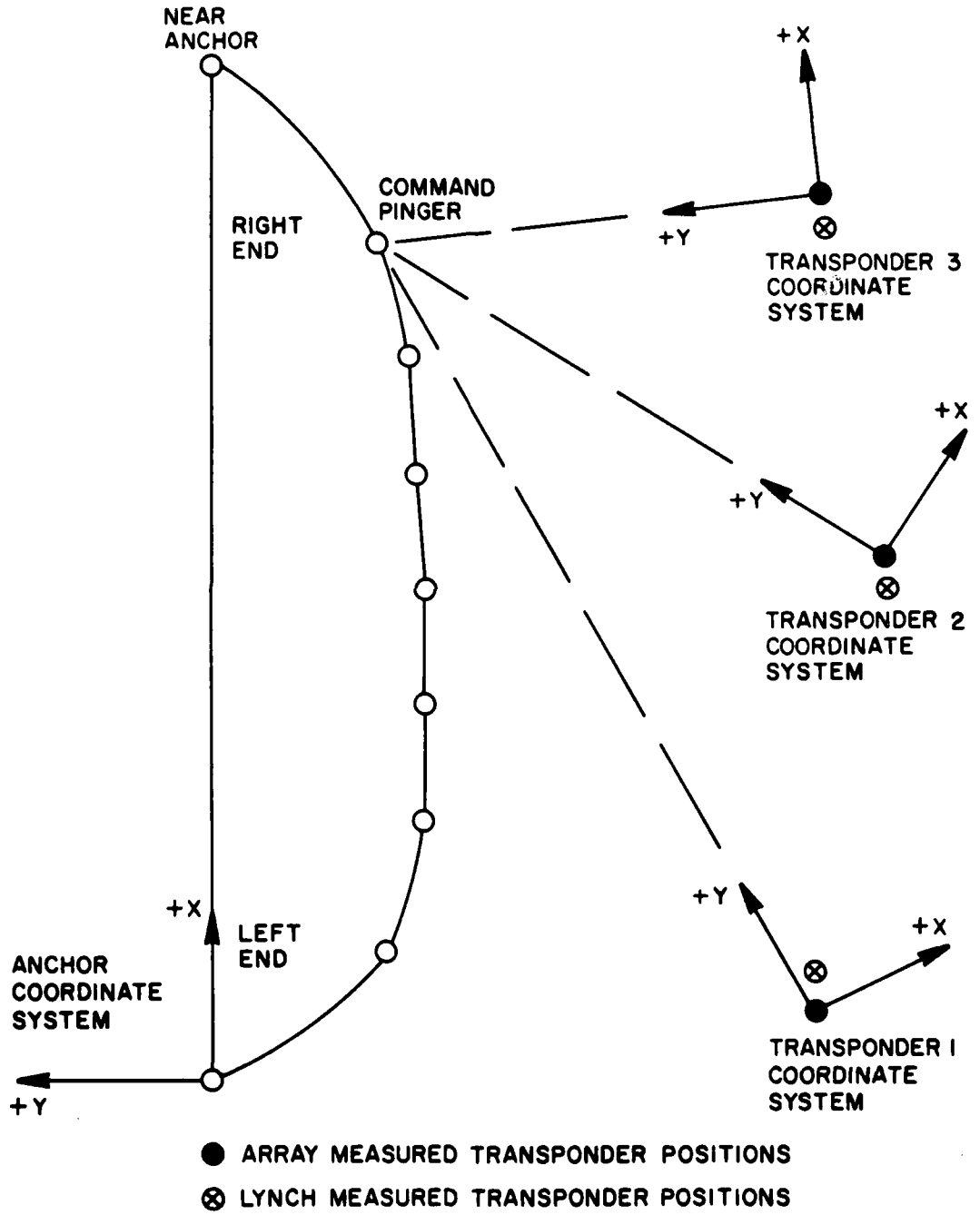

Figure 8. Transponder Coordinate System and the Anchor Coordinate System

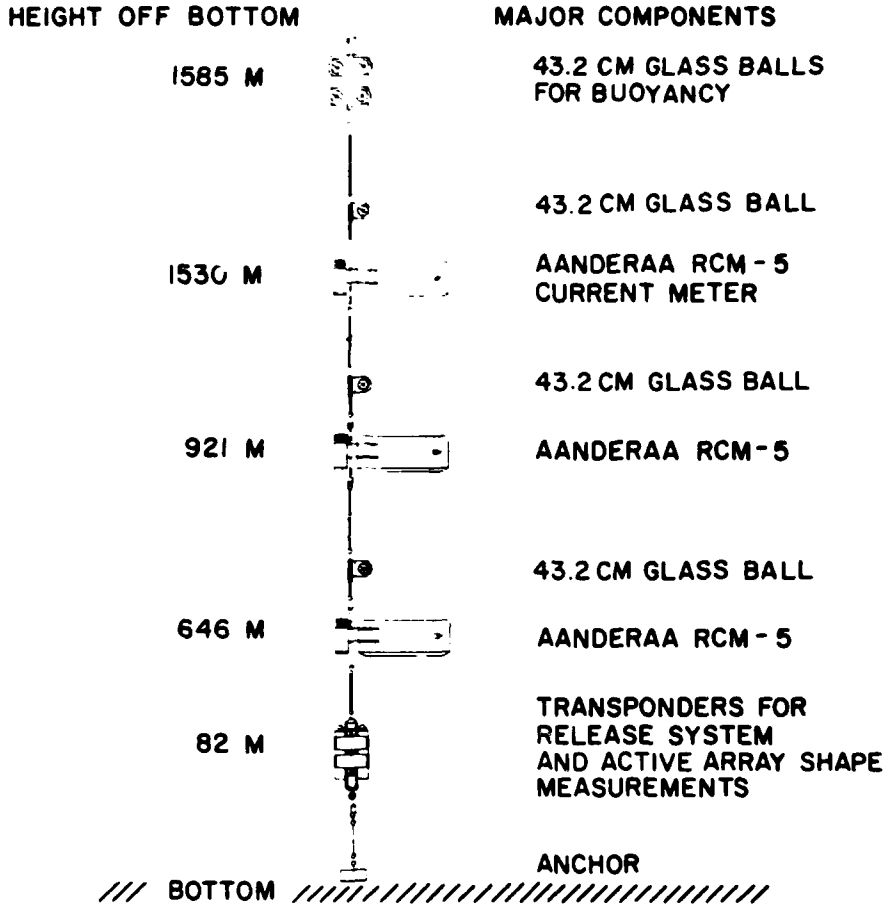

Figure 9. Current Meter Array Configurations

TOP, MID, or BOT; so, for example, the meter at a height off the bottom of 1530 m on EA 1 would be designated EA1TOP. The sample rate was 5 min. In addition to current speed and direction, each current meter also measured temperature and pressure. The current meter sensor characteristics provided by the manufacturer are given in table 5.

Table 5. Sensor Characteristics of Aanderaa Current Meter

	Range	Resolution	Accuracy
Speed	0 to 125 cm/sec	0.1 cm/sec	0.5 cm/sec
Direction	0 to 360°	0.03°	5°
Temperature	-2 to 20°C	0.02°C	0.1°C
Pressure	0 to 562 kg/cm^2	0.549 kg/cm^2	5.62 kg/cm^2

4. RESULTS

4.1 Measured Cable Shape

A scatter diagram of the x/y coordinates of the position sensors for the entire experiment is shown in figure 10. Inspection of the figure shows that the scatter is not symmetrical about sumed anchor baseline. This is probably due to an error during the survey of the anchor locations. Other acoustic sensors on the cable were used to determine the bearing to a distant sound source. That data indicated an error in the anchor baseline of a degree or two. In order to correct for this, a least squares regression line was calculated for the data. The slope of the regression line was 1.5°. The shape data has been corrected by this amount.

From figure 10 one can see that the maximum excursion of the array in the y direction was ±100 m, while the maximum excursion in the x direction was ±25 m.

In order to obtain an intuitive idea of the processes taking place, an average transverse component of the motion of the horizontal span was formed. The average was plotted as a time series in figure 11. The average was formed from the y component of position of the four position sensors near the middle of the span. The data are not taken at uniformly spaced times, so to get a curve for comparison purposes a spline curve was fit to the data.[48] The interesting feature of this plot is that the oscillations were about ±100 m with a periodicity of about 12 hr. The excursions were larger toward the end of the time series corresponding to the time that the currents swung around more nearly broadside to the

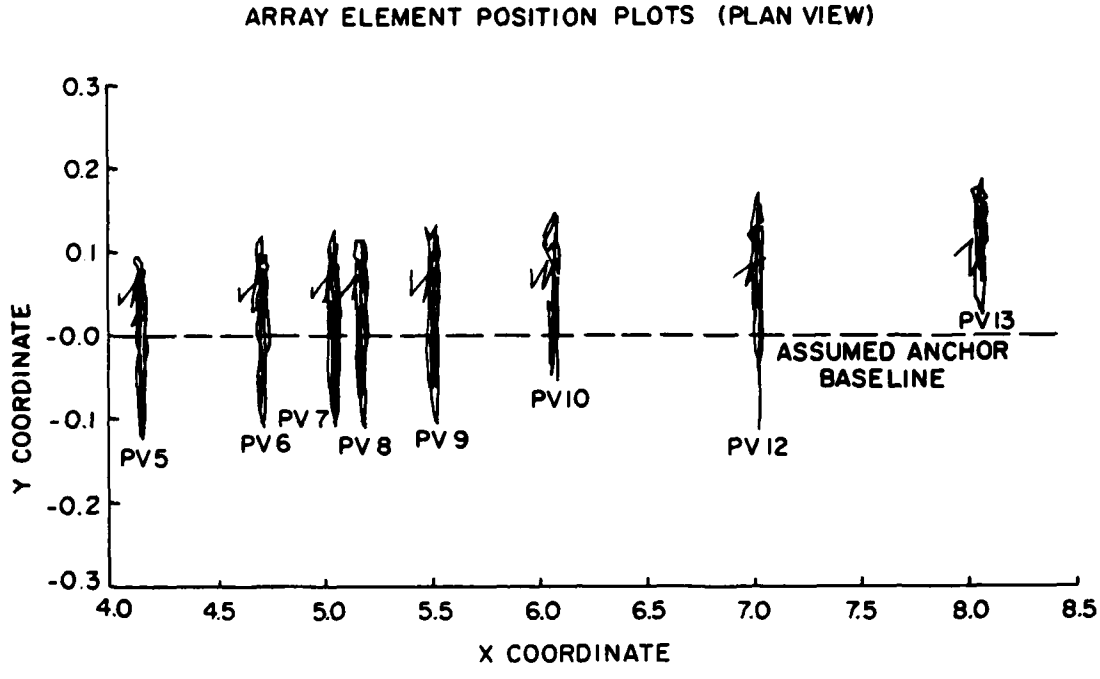

Figure 10. Scatter Diagram of Position Sensors

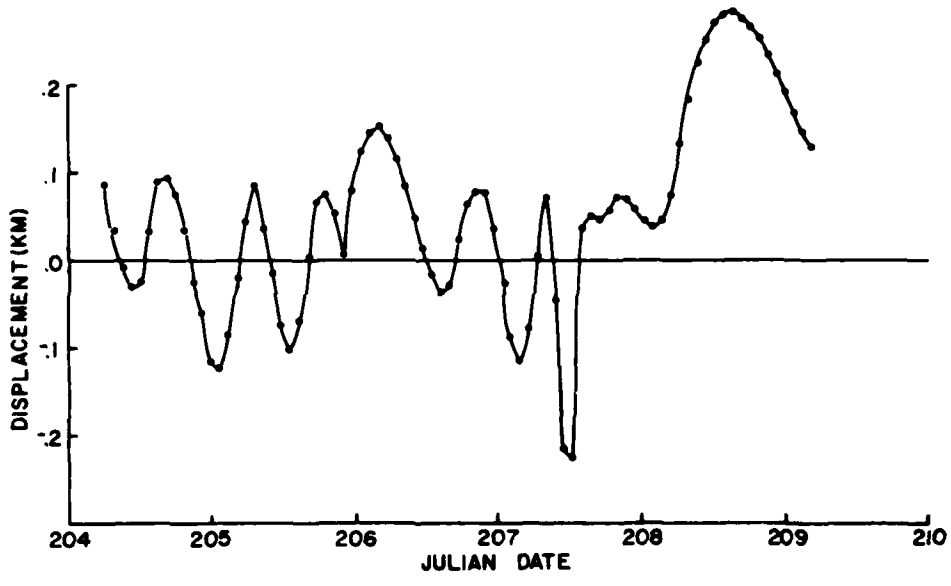

Figure 11. Time Series of Average Position of Cable

cable. Times on the plots are given in Julian date (a table for conversion of Julian data to calender date is given in appendix A).

Similar averages were formed for the x and z components. These data were further analyzed using a maximum entropy technique.[49] This technique is particularly applicable to spectral estimation from short records. It avoids many of the windowing problems that occur when dealing with a finite data set. It is also useful for dealing with records that have missing or bad points. What the technique does is to create an autocorrelation function which is extended beyond the normal limit of lag values using a predictive filter. The power spectrum is then calculated from the autocorrelation with much reduced influence of end effects caused by the short initial time series. The spectra that result from this analysis are shown in figure 12. The peak in the x and y component occurs in the bin centered around 12.2 hr period. There is only a small peak in the z component motion.

There were three pressure sensors included along the cable. The sensor designated D1 was colocated with the command pinger. Sensors D2 and D3 were near the middle of the cable. The sensors D2 and D3 were observed to drift considerably during pressure testing. The problem was detected too late to change the sensors before the system was deployed. They cannot be considered reliable. Sensor D1, however, did not exhibit the same drift characteristics. Its output is considered reliable. The output from each pressure sensor was converted to depth and then plotted as height above the sea floor. The resulting plot is shown in figure 13.

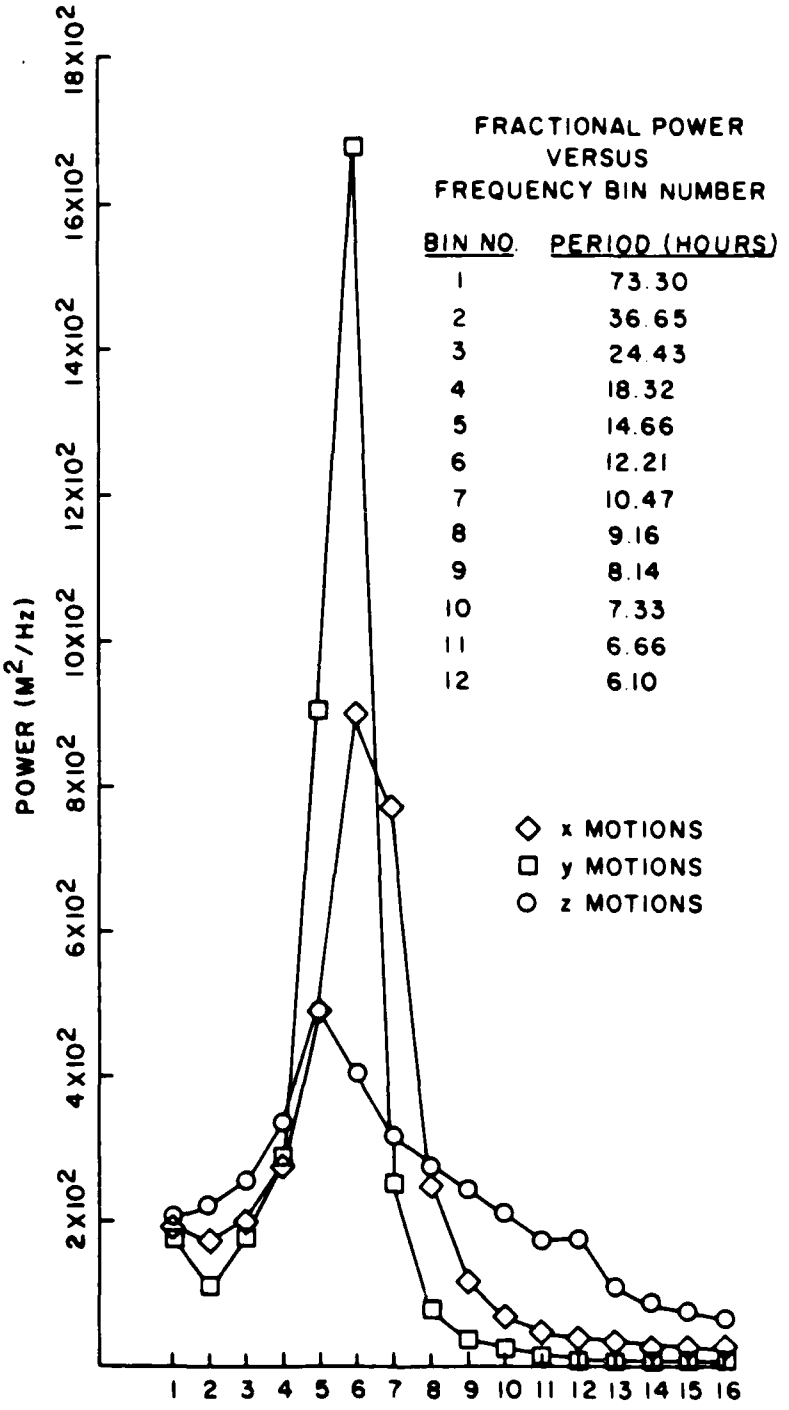

Figure 12. Spectra of X, Y, Z Component of Average Cable Displacement

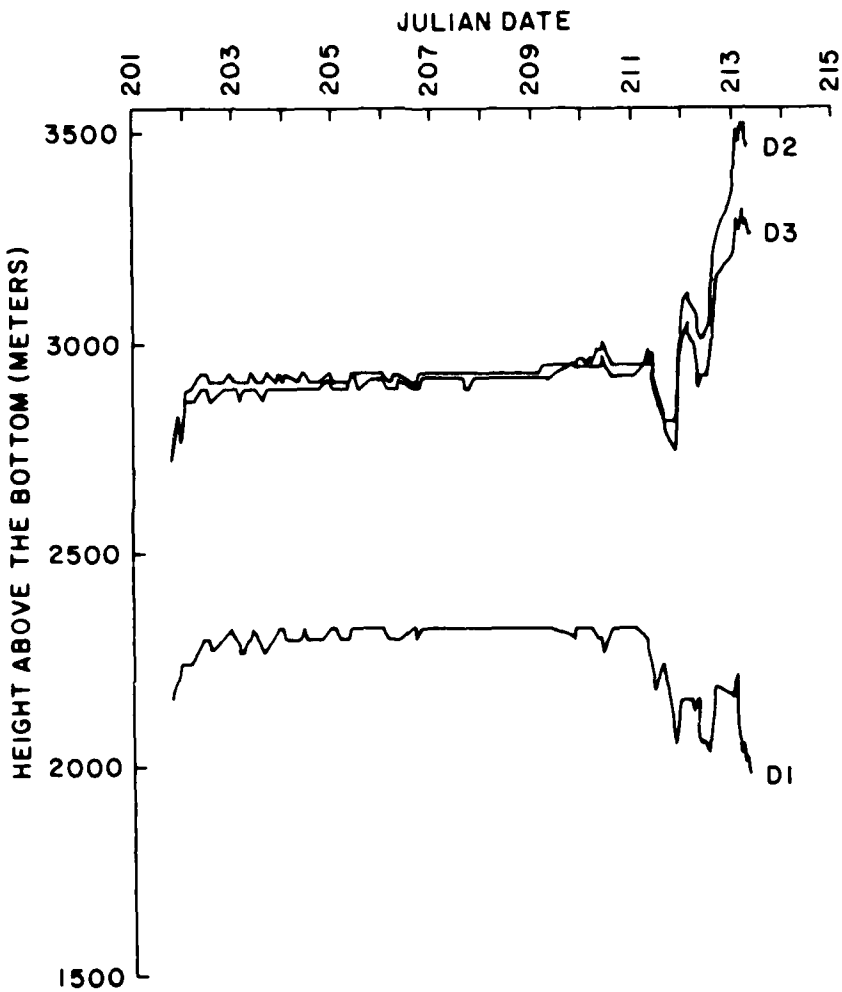

Figure 13. Depth Sensor Output

The height measured by sensor D1 was in agreement with that calculated for the command pinger to within the resolution of the depth measurement. The resolution was 30 m.

There is a large depth excursion beginning on Julian day 211. During this time the umbilical cable became fouled in the riser. None of the data from this period was used in this analysis.

The cable shape observations chosen for analysis are shown in figures 14 to 19. The observations are broken down into two periods. The first period, designated run 1, covers the period 0701 to 1311 on day 205. During this time the cable moved from a southerly position to a northerly position. The second period, designated run 2, covers the time from 1343 to 1833 of day 205. During this time the cable moved from a northerly position to a southerly position.

4.2 Sources of Error in Cable Shape Measurement

The position sensors did not always receive signals from all possible paths and, in addition, under conditions of low signal-to-noise ratio, some sensors did not immediately make a detection. Missing pings were detected by sorting arrivals by ray paths, but the second error, the delayed detection, was more subtle and data flawed by this error was sometimes included for analysis. In order to find this flawed data, a check of the calculated straight line distance between adjacent sensors was performed. If the distance between the sensors calculated from the data was greater than the known distance along the stretched cable, then one of the two points was bad. The bad one was determined by performing a similar check using combinations of adjacent sensors.

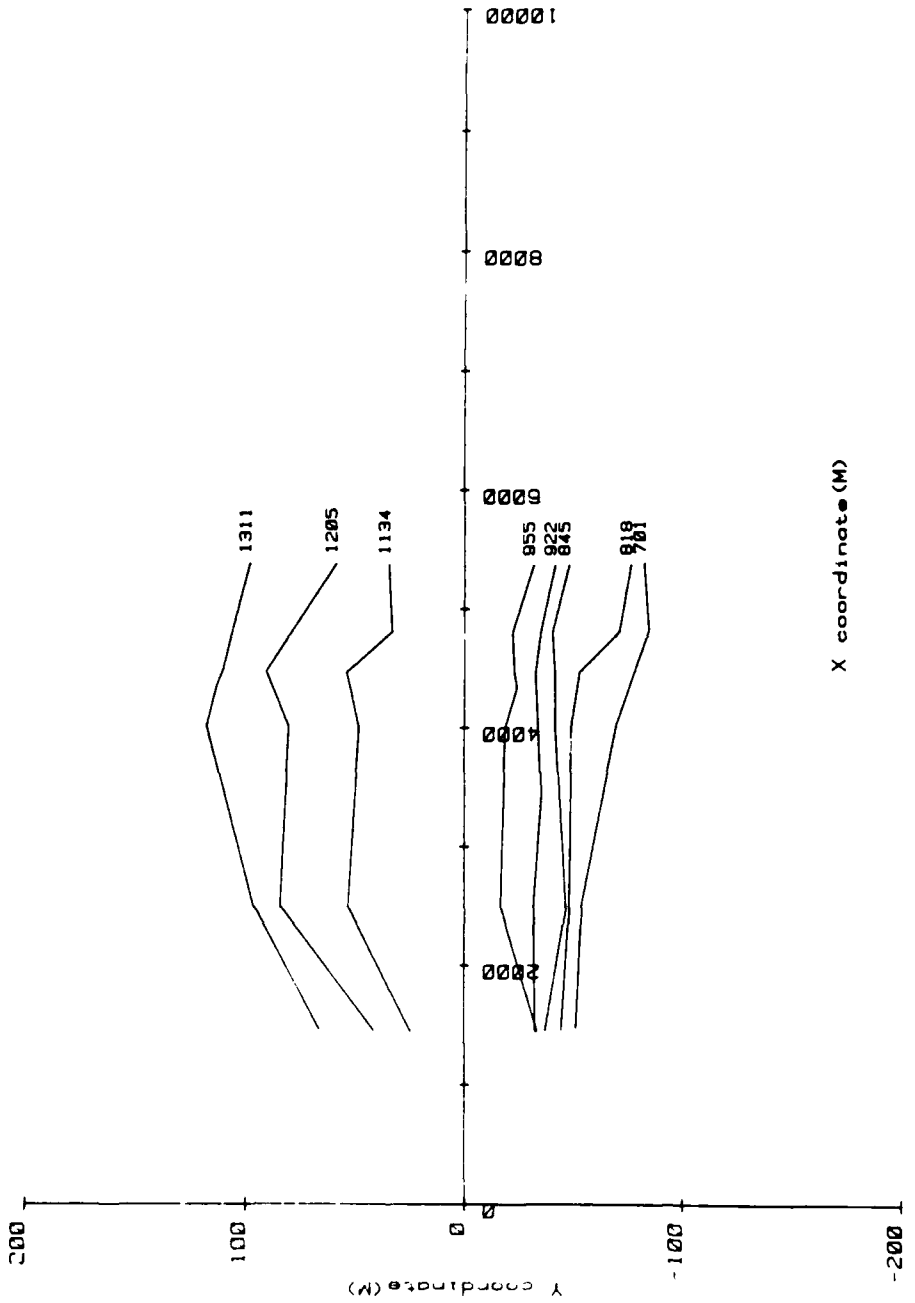

Figure 14. Observed Cable Shape Projected on XY Plane, Run 1

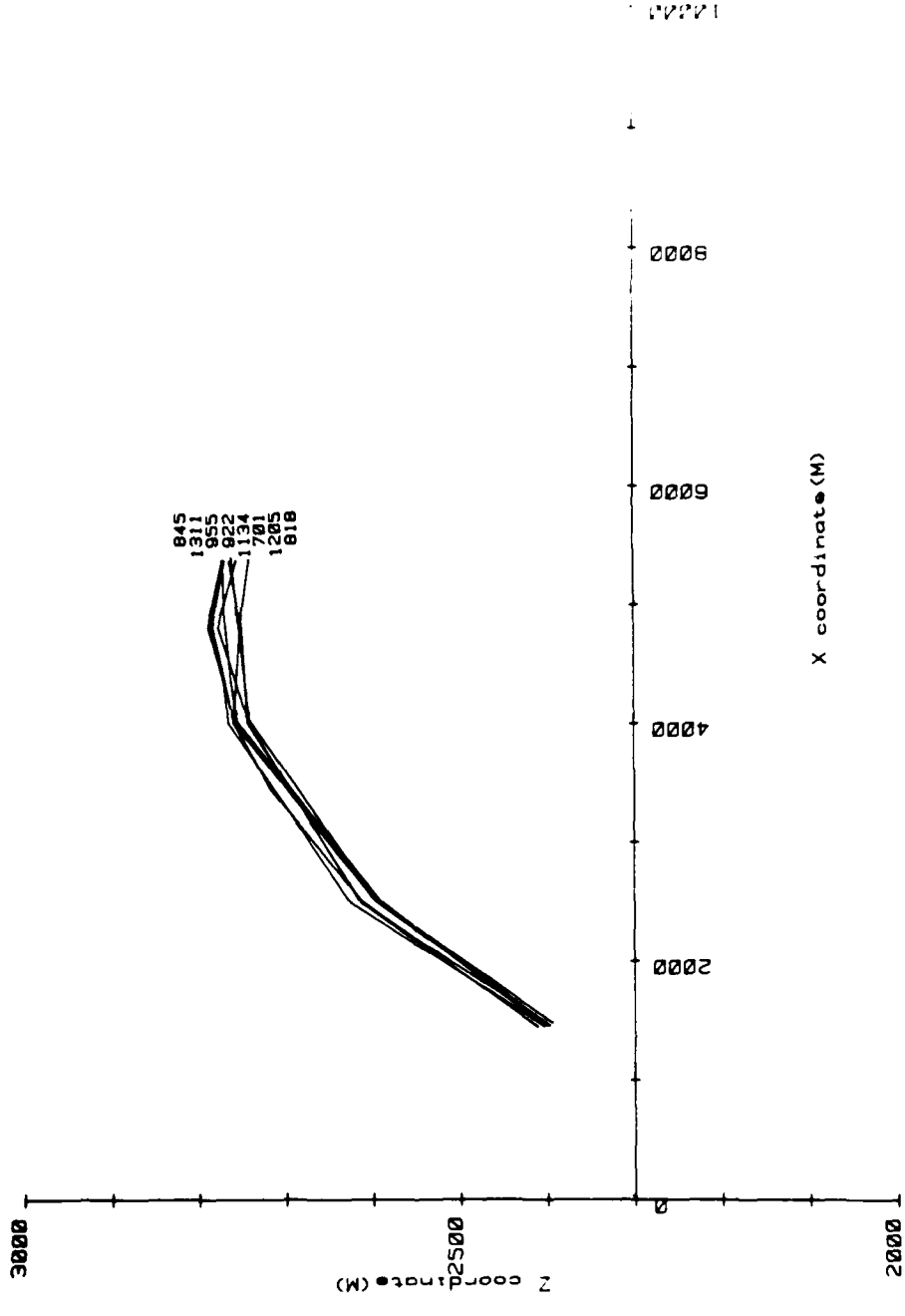

Figure 15. Observed Cable Shape Projected on XZ Plane, Run 1

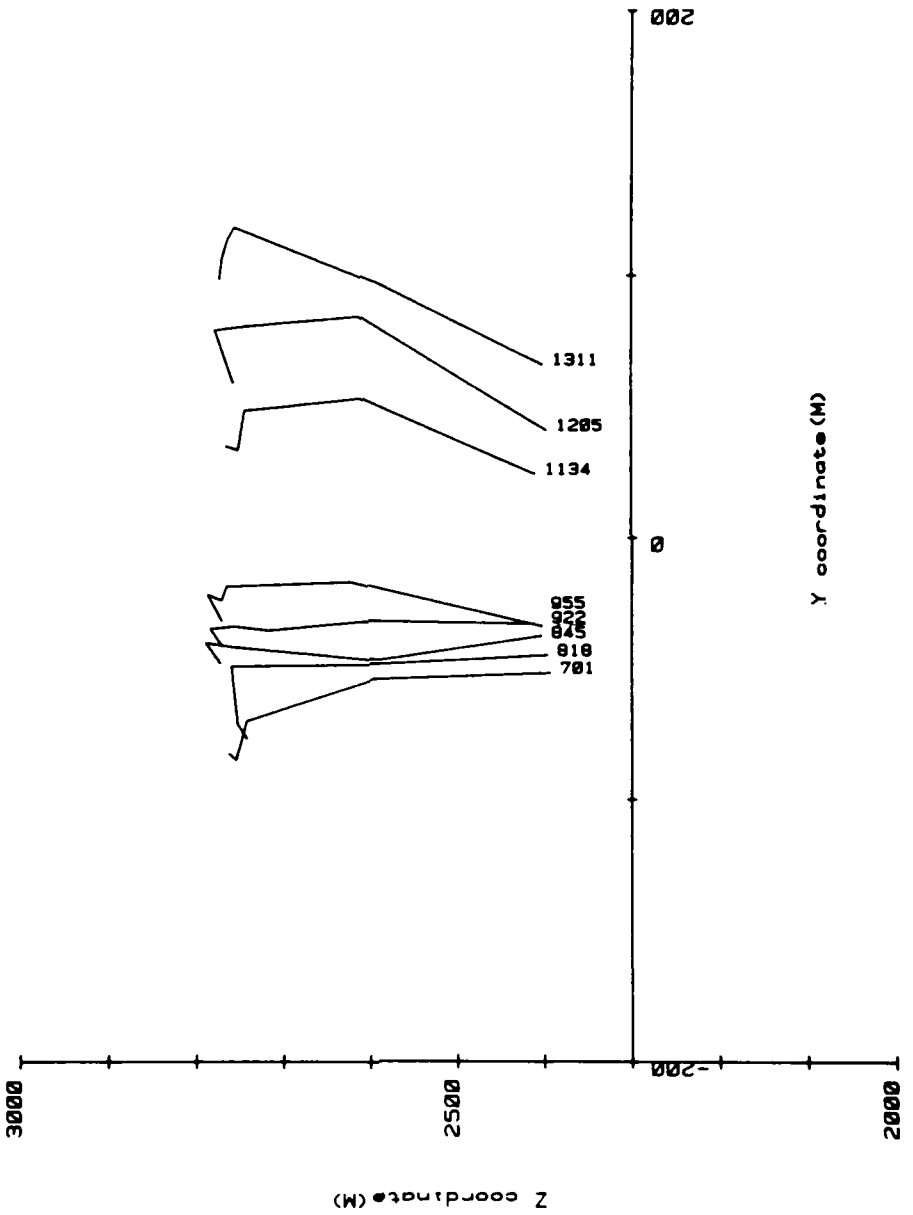

Figure 16. Observed Cable Shape Projected on YZ Plane, Run 1

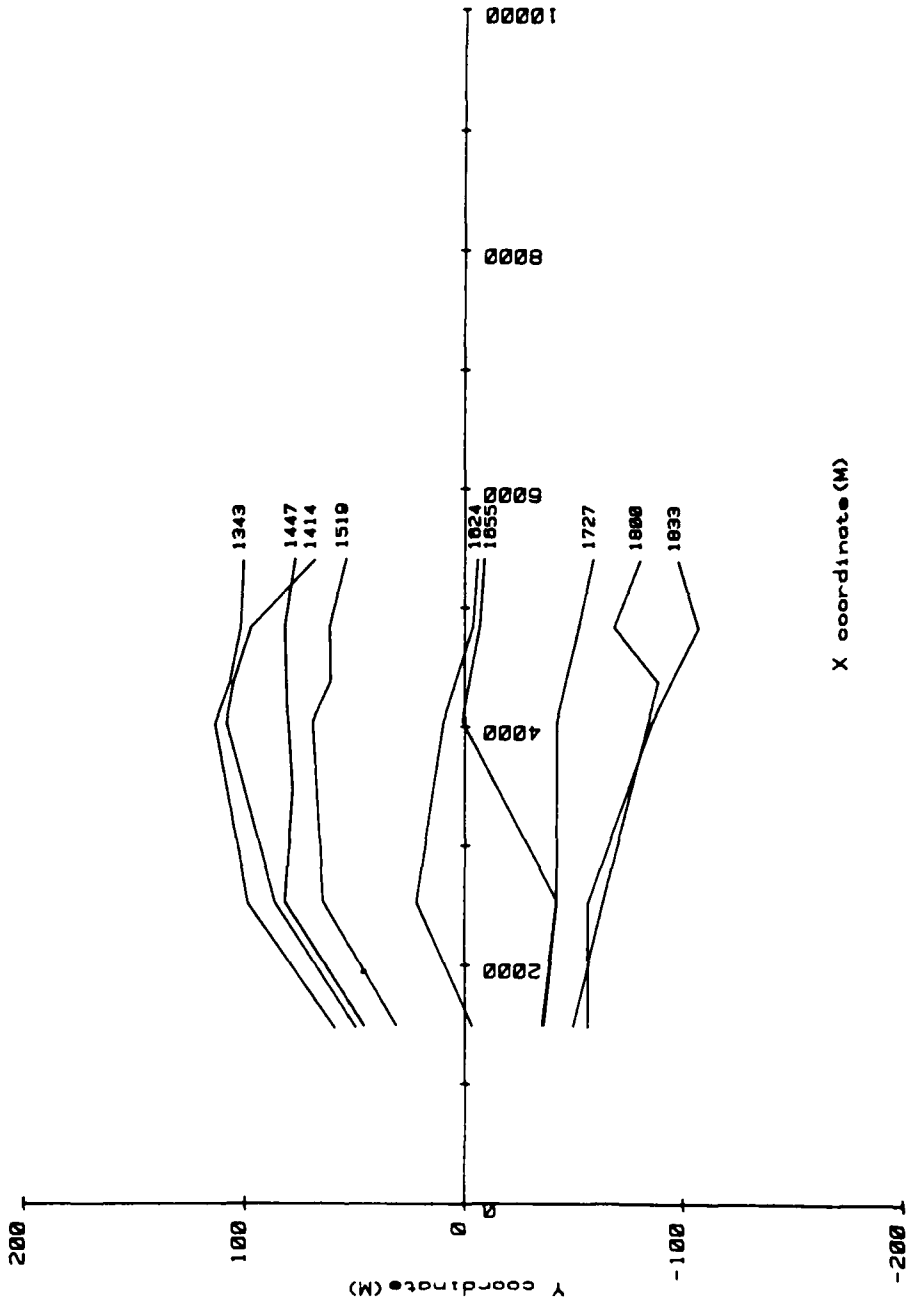

Figure 17. Observed Cable Shape Projected on XY Plane, Run 2

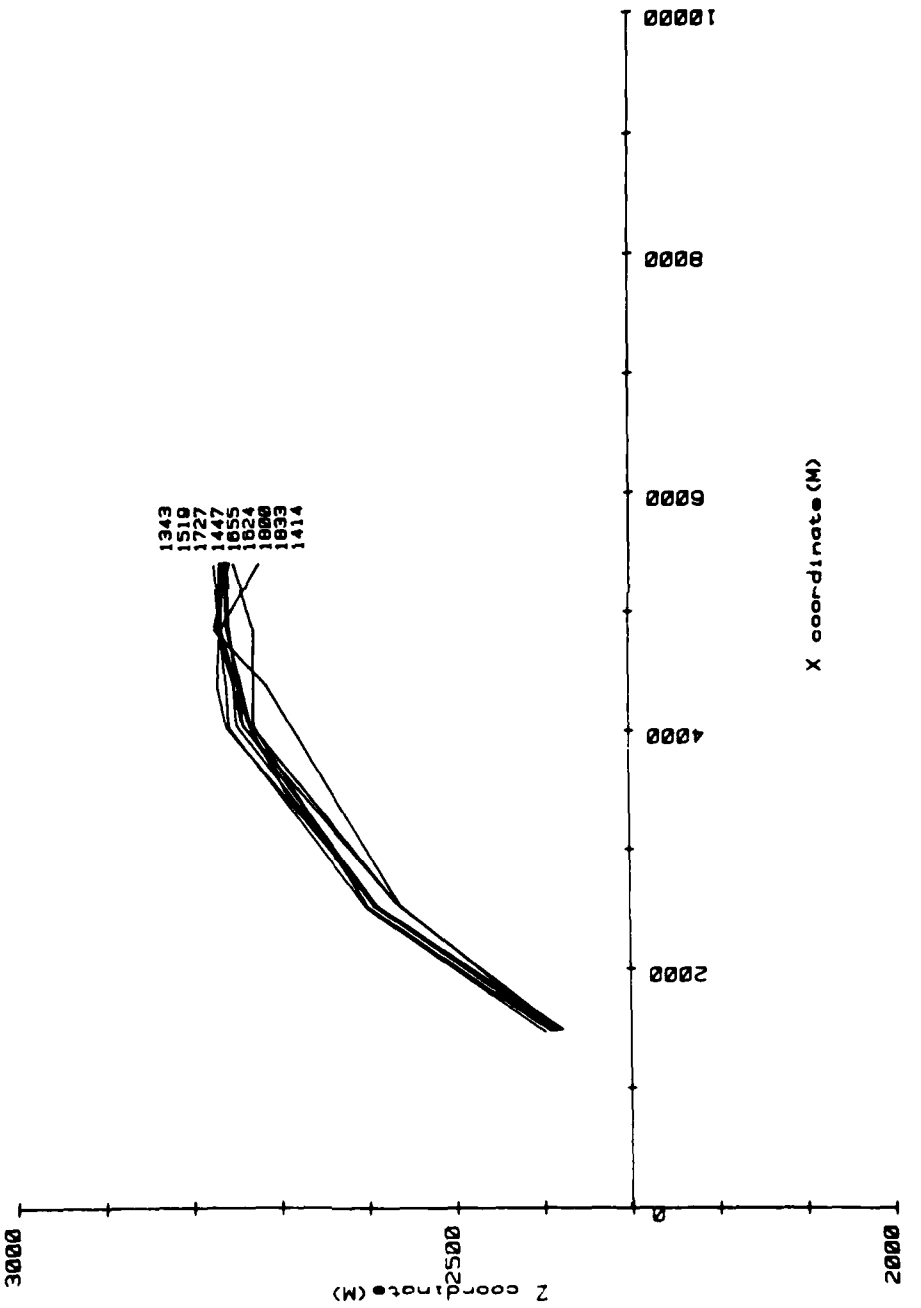

Figure 18. Observed Cable Shape Projected on XZ Plane, Run 2

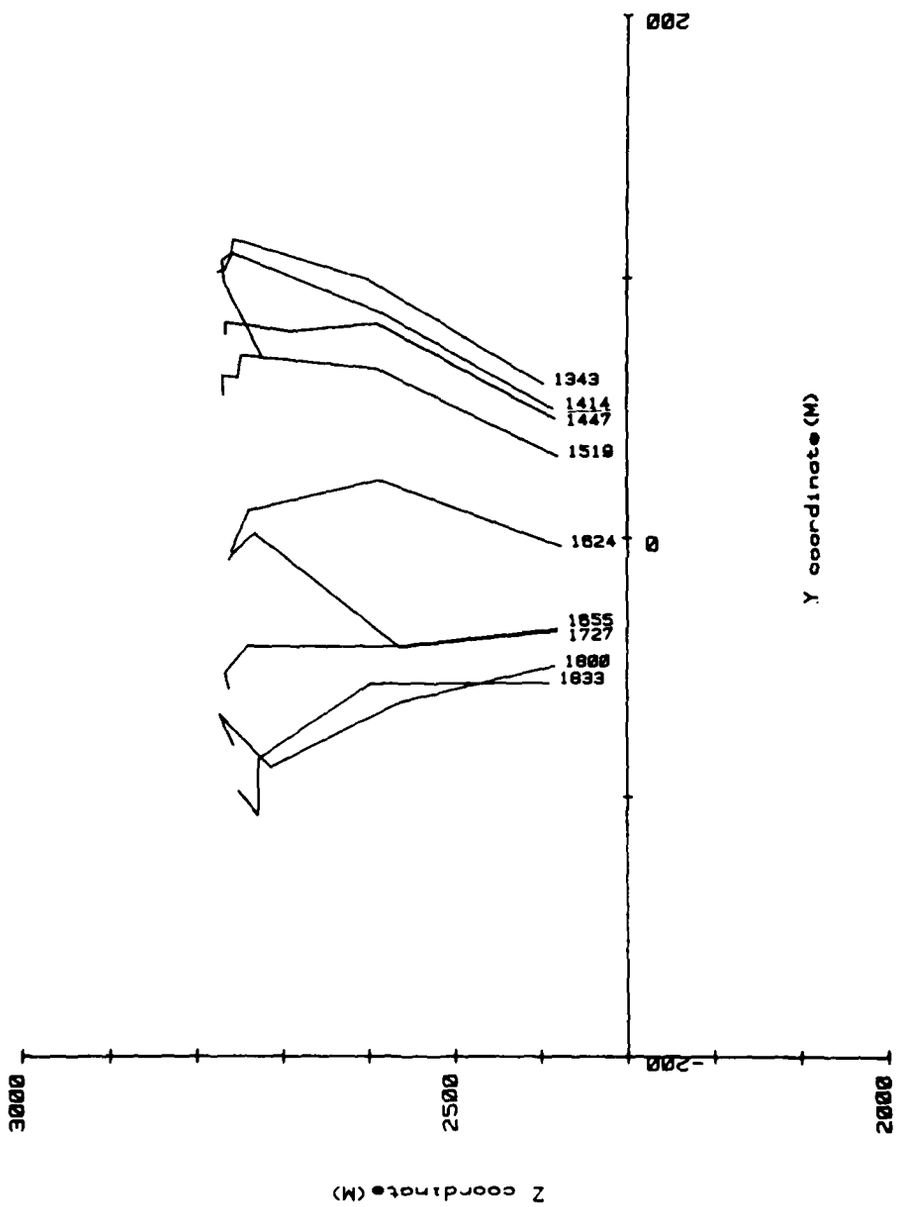

Figure 19. Observed Cable Shape Projected on YZ Plane, Run 2

Travel time was converted to distance under the assumption that the acoustic rays travel in straight lines. It is known that sound in the presence of a sound velocity gradient will travel along a curved path which minimizes the travel time in accordance with Fermat's principal. In order to examine the magnitude of the error from this assumption, an experiment was set up using the Generic Sonar model.[50] The geometry of the experiment is shown in figure 20. This geometry is representative of the geometry of the ray paths between the acoustic source on the array and one of the reference transponders.

Eigenrays connecting the source and receiver were calculated using the Generic Sonar Model. One of the model outputs was travel time along a ray. The mean sound speed was calculated by dividing the vertical distance between the source depth and receiver depth by the travel time for a vertical ray.

The straight line distance for the direct path (C) is given by

$$C^2 = (3904.7)^2 + (5484 - 3139)^2 \qquad (46)$$

$$C = 4554.7 \text{ m.}$$

Travel time T_c = 4554.7/1534.59 = 2.9680 sec.

Travel time following a curved ray = 2.9666 sec.

In this case the error due to the assumption that rays are straight lines is 1.4 msec. This corresponds to a slant range distance error of about 2 m.

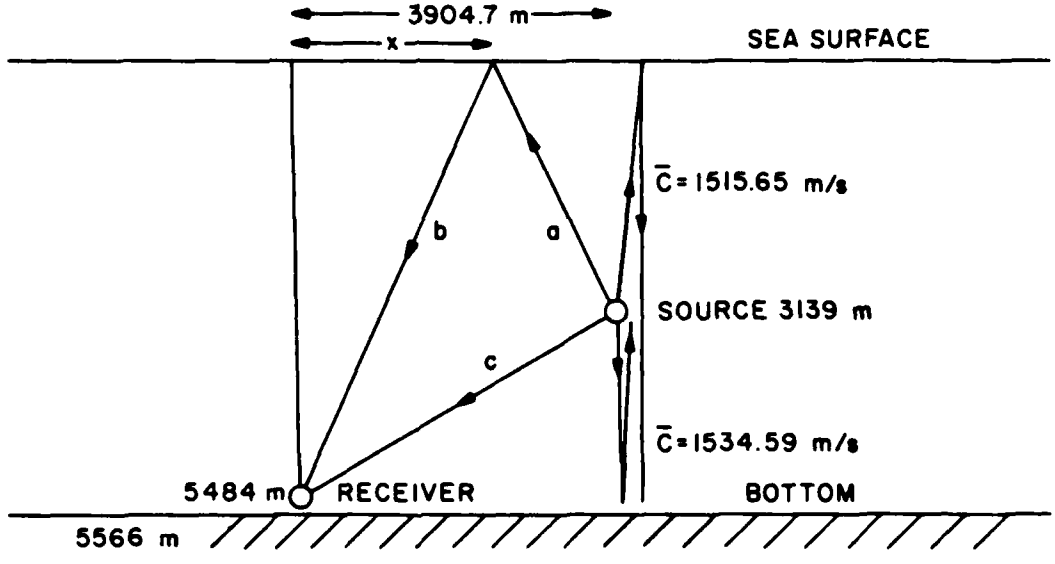

Figure 20. Geometry of Model Experiment to Test the Effects of Ray Curvture on Acoustic Travel Time

The straight line distance for the surface reflected path (a + b) is determined using the properties of similar triangles to obtain simultaneous equations:

$$\frac{3904 - x}{3139} = \frac{x}{5484} \tag{47}$$

$$\frac{3139}{a} = \frac{5484}{b} \tag{48}$$

$$(5484)^2 + x^2 = b^2 \tag{49}$$

Solving this set of equations yields;

$x = 2482.8$ m

$b = 6020.0$ m

$a = 3445.8$ m

Travel time $T_{(a+b)} = 9465.8/1515.65 = 6.2454$ sec.

Travel time following a curved ray = 6.2451 sec.

In this case the error due to the assumption that the ray travels in a straight line is 0.3 msec. This corresponds to a slant range distance error of about 0.5 m. The smallness of the error in this case is probably fortuitous since the accuracy of the eigenray calculation is about 1 msec.

A further source of error in the cable shape measurement comes from the fact that the bottom mounted reference transponders are actually buoyed up from the sea floor to a height of 83 m. The mooring is then subject to action by ocean currents. The result of a mooring deflection

study is shown in figure 21. Under the conditions experienced during the experiment the calculated transponder positions would not be expected to vary by more than 1 or 2 m.

A possible source of error comes from the fact that a single sound speed profile was used for conversion of travel time to distance. Surface heating, mixing processes, water mass advection or internal waves could alter the sound speed profile. A check on errors from this source was performed by adding the round trip travel time from the pinger to the surface to the round trip travel time from the pinger to the bottom. Since the distance from the surface to the bottom was fixed, any important differences in mean sound speed would be reflected in the travel time. The average travel time was determined on three different days and the difference of the averages was tested for significance using student's T test. There was no significant difference in the means at the 0.01 level. Consequently we can say that the changes in the sound speed profile that may have occurred did not produce appreciable changes in the average sound speed used in the conversion from travel time to distance.

4.3 Ocean Current Data

Time series plots of ocean current measurements are presented in figures 22 and 23. The data were corrected for magnetic variation (18°W) and then resolved into components along axes oriented toward North and East. The component data were then filtered with a lowpass Butterworth filter (1 pole). The high frequency cutoff for this filter was 1 cycle/hr. The data were then resampled at half hour intervals. In order to obtain the data set presented in the figures, a further rotation was made to a heading of 125°T, the nominal line of bearing of the line

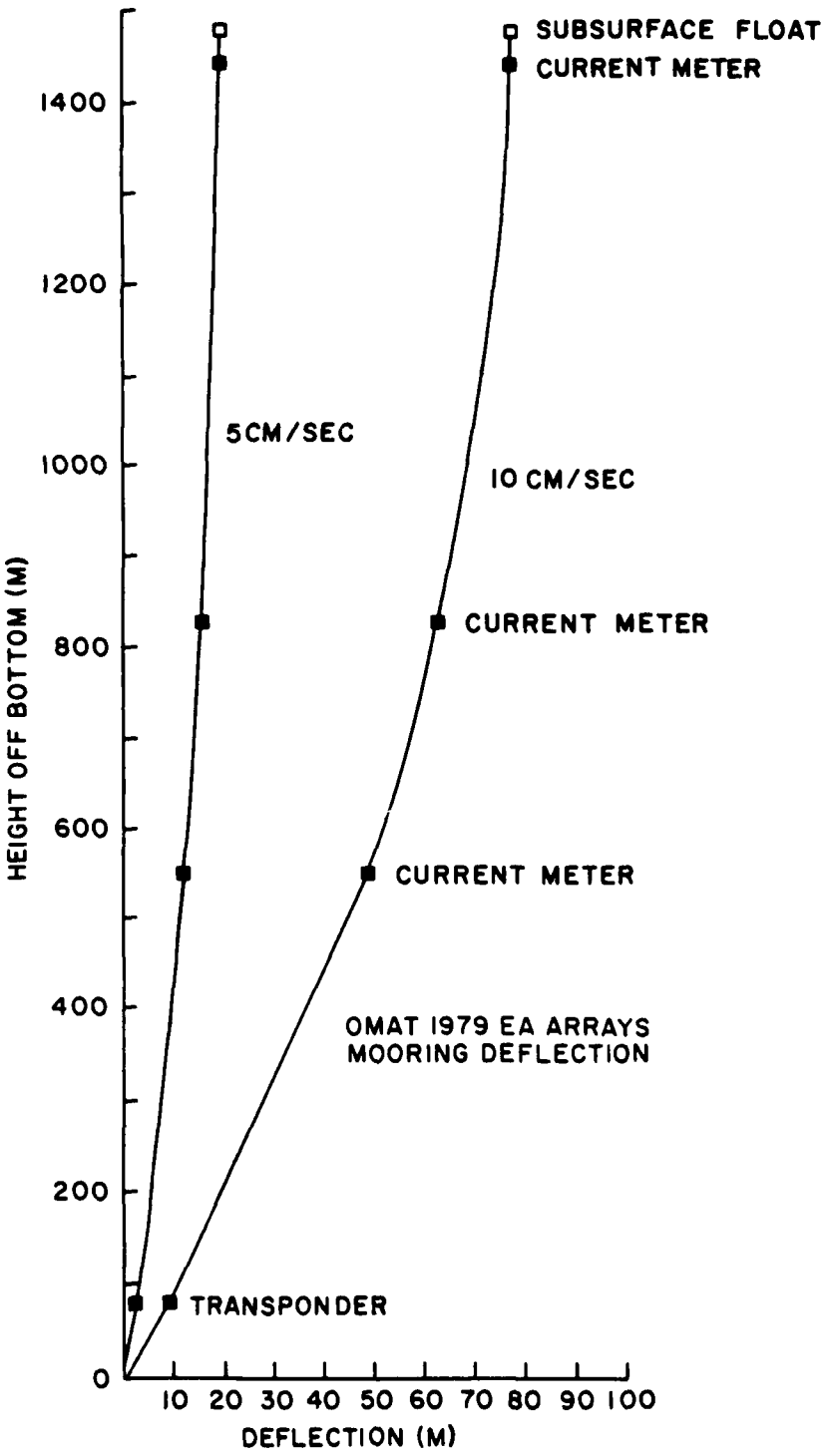

Figure 21. Transponder Array Deflection in Ocean Currents

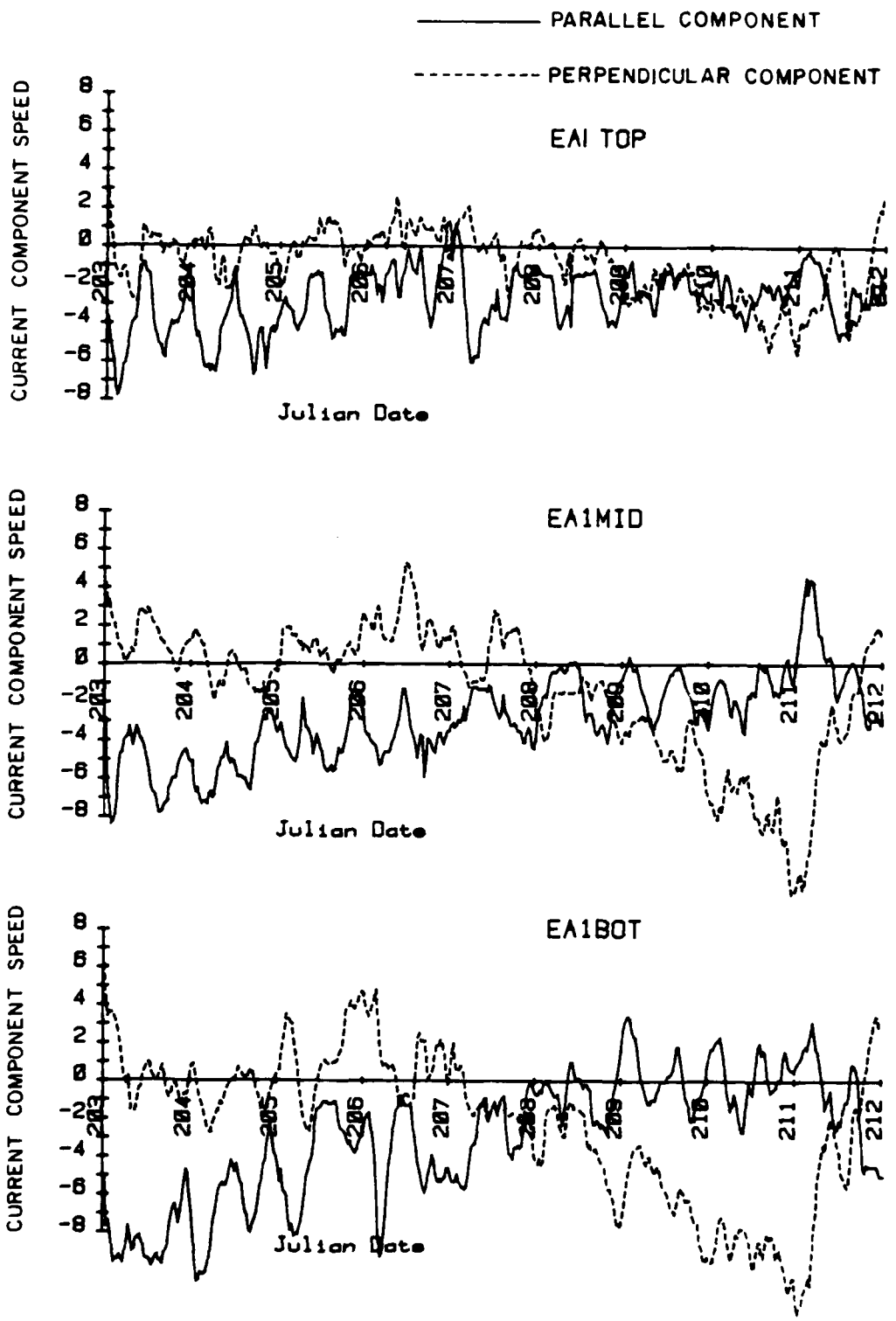

Figure 22. Time Series of Current Components Normal and Parallel to Cable from EA 1

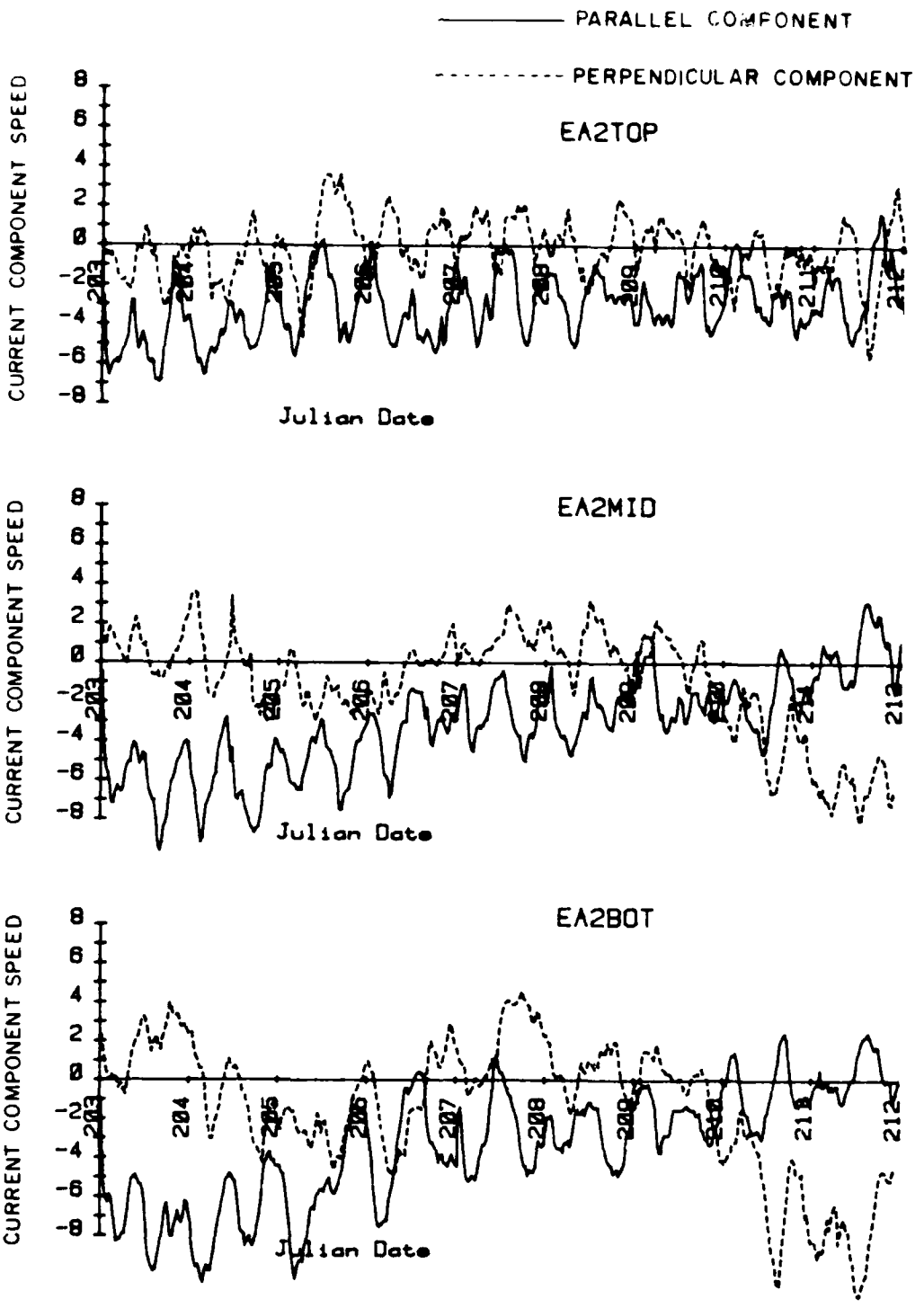

Figure 23. Time Series of Current Components Normal and Parallel to Cable from EA 2

connecting the two cable array anchors. Here a positive parallel component is toward 305°T; a positive perpendicular component is toward 035°T.

This same data set is plotted on a progressive vector diagram in figures 24 and 25. At measurement site EA 1 the currents up to 26 July (Julian day 207) are generally in a direction of 116°T. The currents then swing south for a day then to the southwest. This process begins a day later on 27 July (day 205) for the middle current meter. At measurement site EA 2, the currents are generally the same at all three levels in a direction of 120°T. Then on 24 July (day 210) the currents at the two deeper meters turn toward 140°T while the top meter continues to show currents toward 120°. On 26 July currents at the two deeper meters swing back toward 100°T. Not until 29 July do the two deeper meters indicate a current swing to the south, three days later than the similar event at station EA 1 (remember that the horizontal separation of the two arrays is only about 4 km).

It is interesting to note that these data are inconsistent with the general circulation model of the North Atlantic of Worthington.[51] Worthington's model predicts westerly currents at a depth of 4000 m at the measurement location. Owens and Hogg[52] reported similar anomalies in current measurements made near a bathymetric "bump" of similar dimension to the "bumps" in the vicinity of these current measurements.

Power spectra of the current magnitude were calculated for each meter. The spectra are shown in figures 26 and 27. All spectra have a peak at about 0.08 cycle/hr, which corresponds to a period of 12.5 hr.

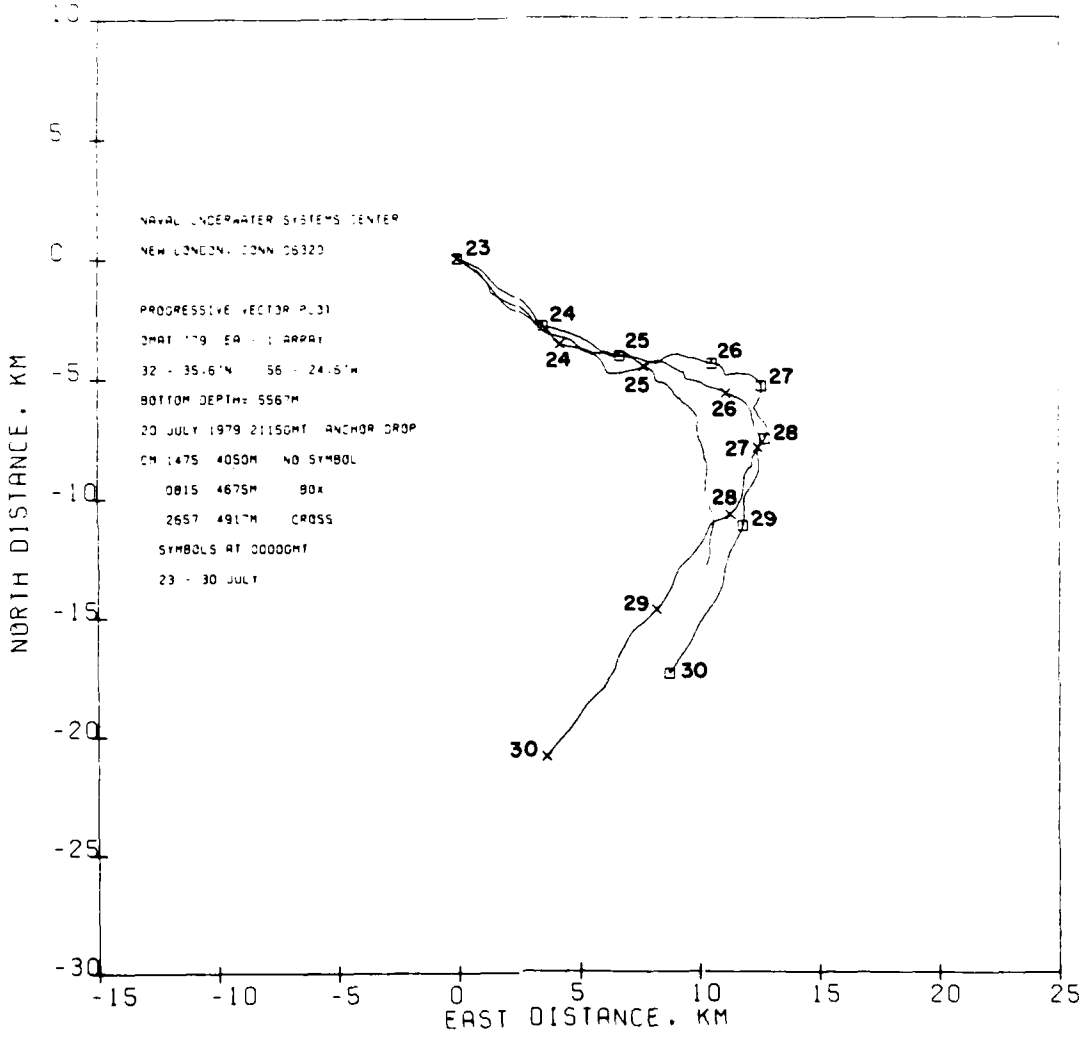

Figure 24. Progressive Vector Diagram for Current Meters on EA 1

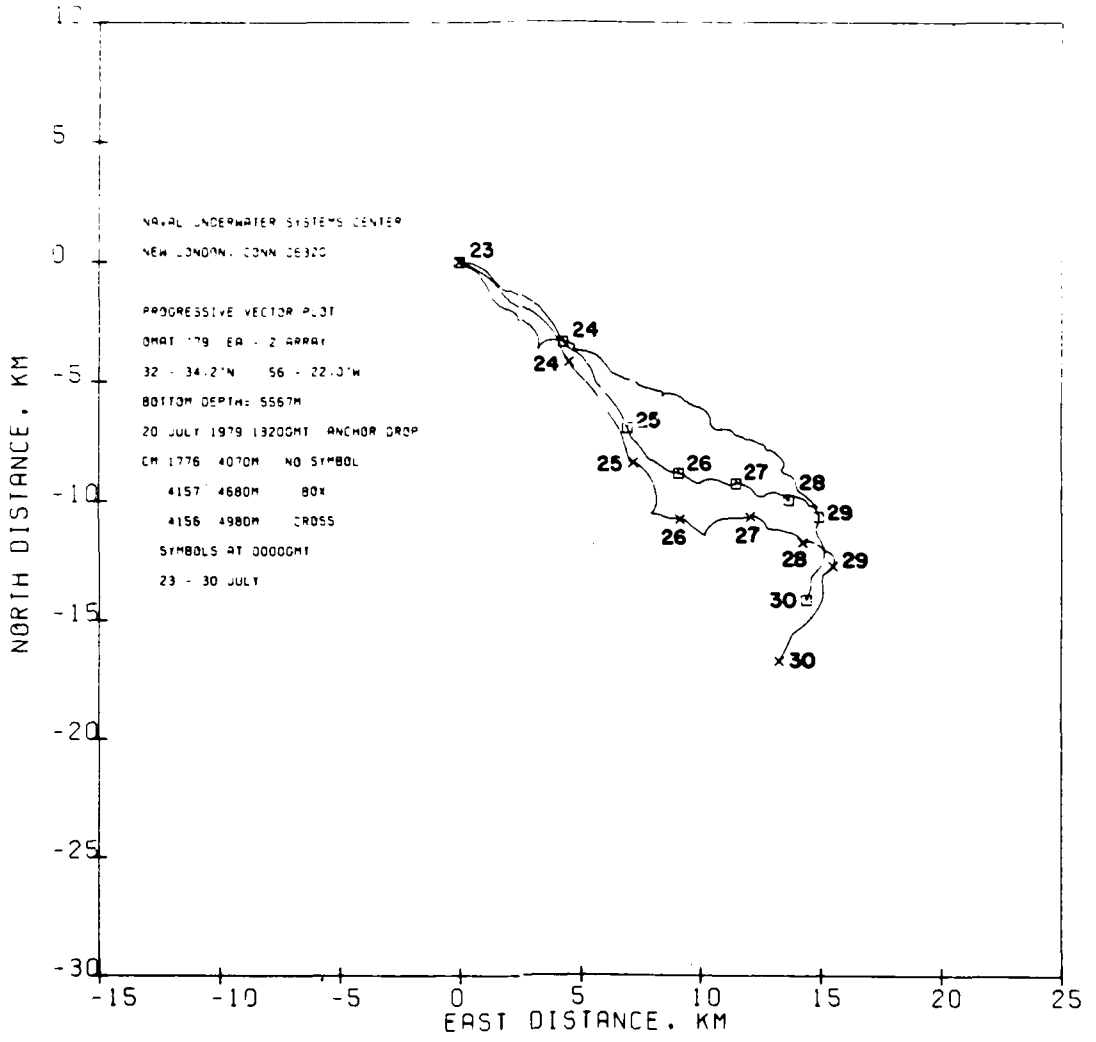

Figure 25. Progressive Vector Diagram for Current Meters on EA 2

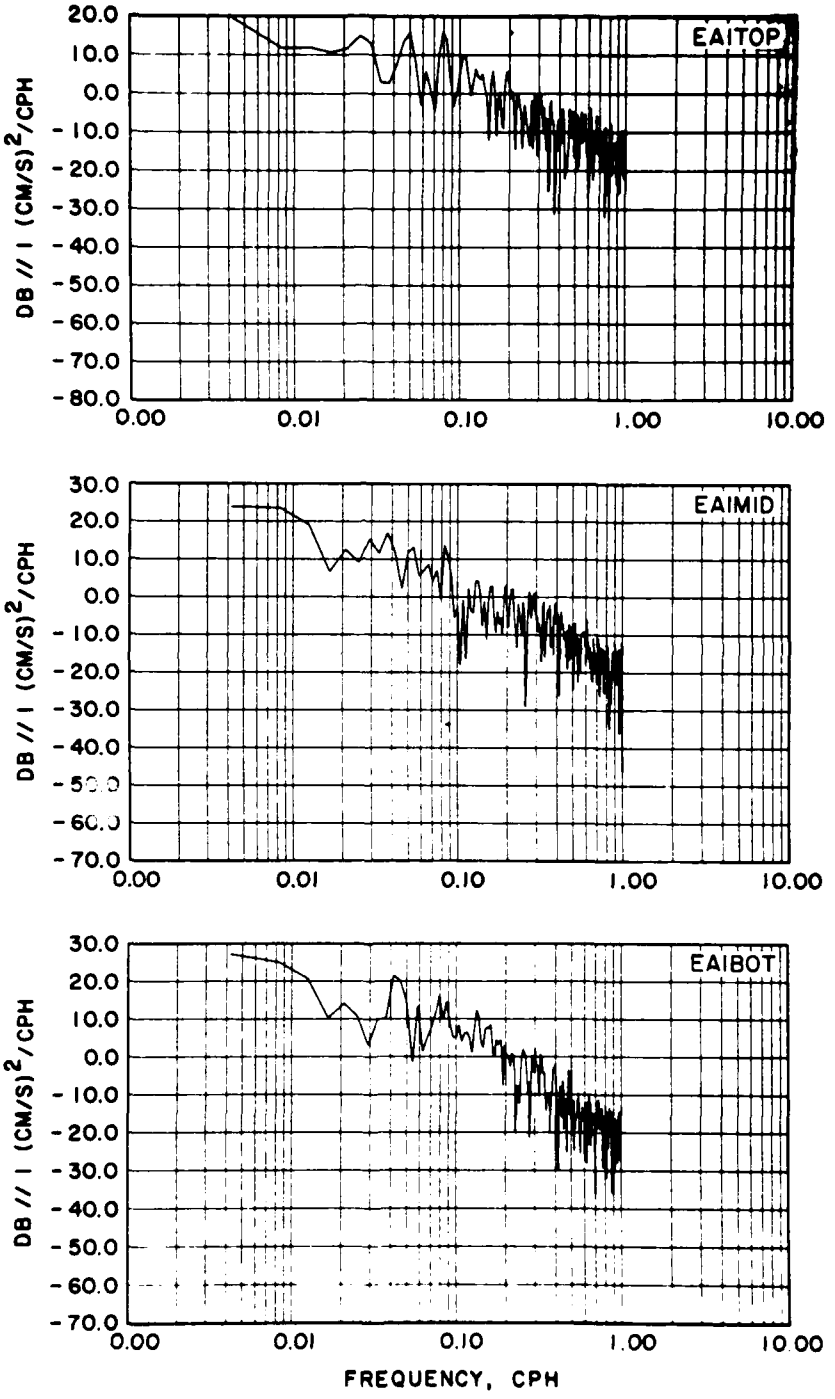

Figure 26. Current Magnitude Spectra From EA 1

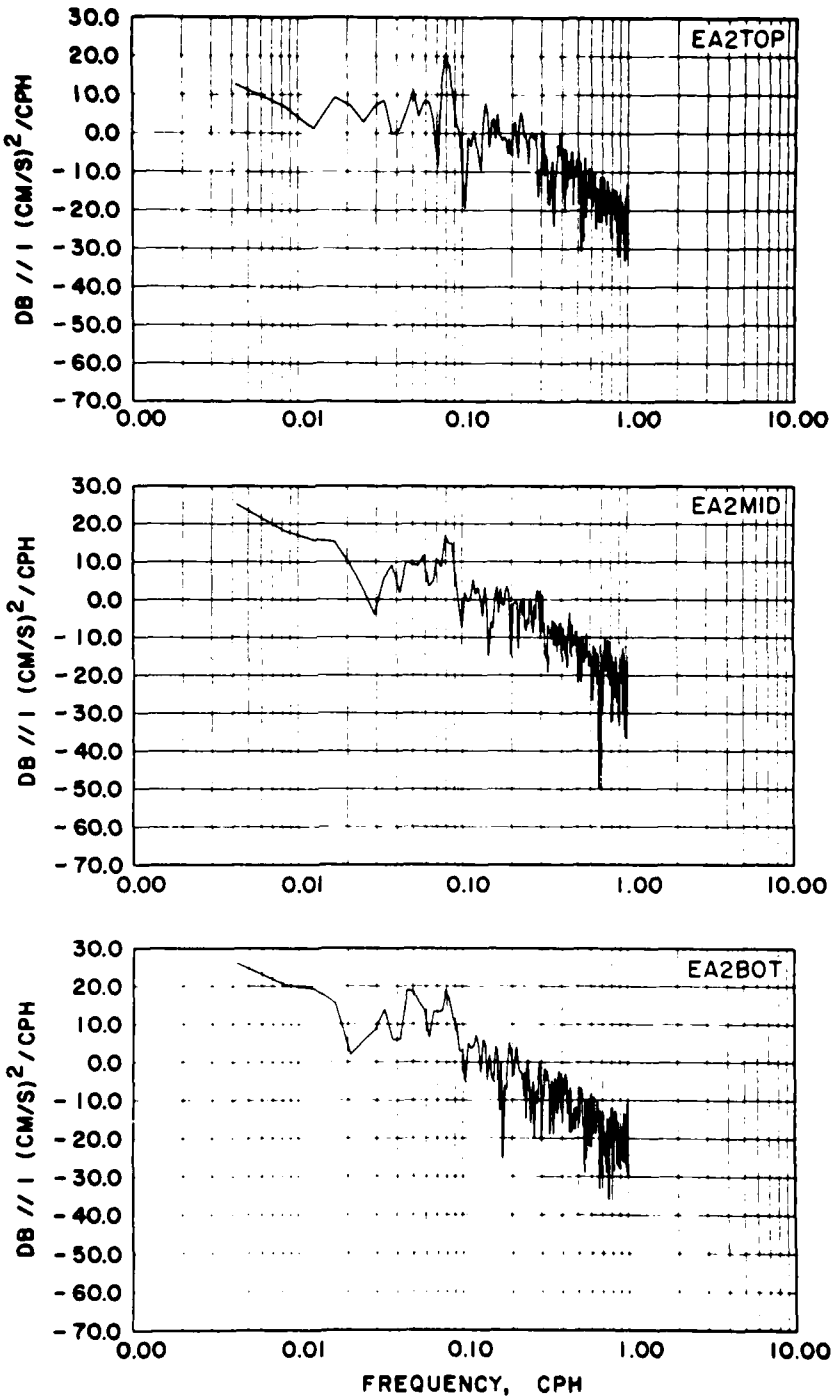

Figure 27. Current Magnitude Spectra from EA 2

At the latitude of the measurements the inertial period is 22.3 hr. The period of the M_2 constituent of the tide is 12.42 hr.[32]

4.4 Static Models

Two static models were investigated. The DESADE model was of the imaginary reaction type, the GRIFFIN model solved the steady state differential equations and used the imaginary reactions for determining the boundary conditions.

The most widely used static model is the DESADE model developed at the Naval Research Laboratory.[14,15] The model considers only the normal component of the drag force and in its original version permitted ocean current variations only as a function of depth. The most significant modification of the program by other users is in the provision for complicated current fields which vary in the horizontal as well as in the vertical.[53,54] The principal limitations of the model from the point of view of the present study are that the cable structure cannot consist of more than 22 segments and the neglect of tangential drag. Provision has been made to introduce a strum amplified drag coefficient which is a function of Reynolds number.[34] Plane and side views of the DESADE output for various current speeds broadside to the cable are shown in figures 28 and 29. Listings of the data are provided in appendix B. Additional runs were made for several values of the drag coefficient. The maximum deflections of the cable by currents of 2.5 cm/sec are shown in table 6 for various values of the drag coefficient. The effect of changing the drag coefficient can be dramatic, as seen (for instance) in figure 30. This is a plot for the strum amplified drag coefficient calculated according to Skop and Rosenthal.[34]

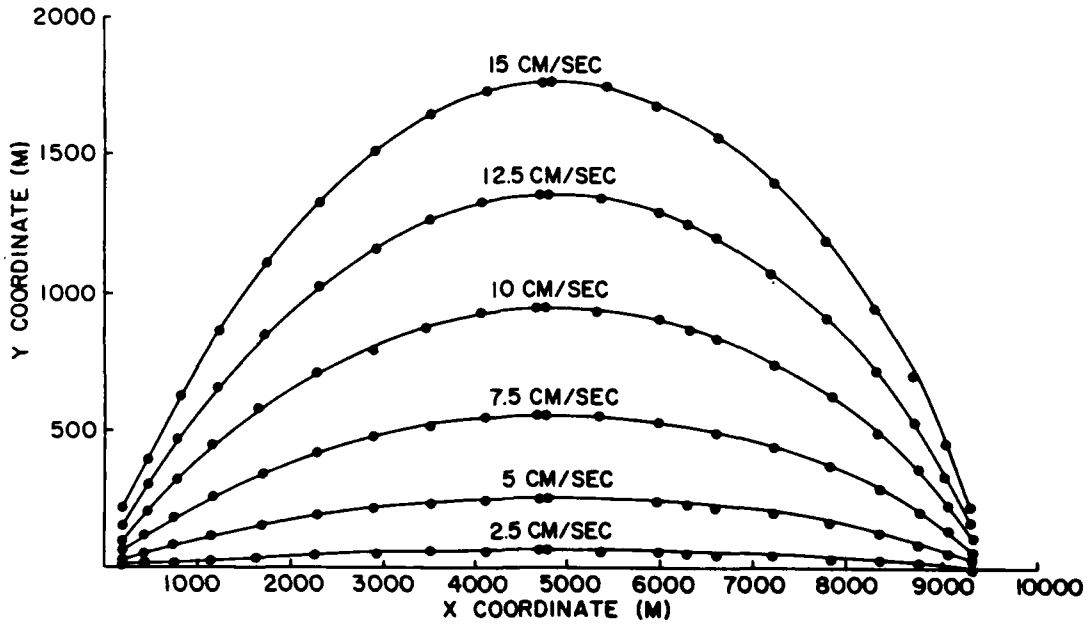

Figure 28. Plan View of Cable Configuration Calculated by Static Model for Currents of 2.5, 5, 7.5, 10 cm/sec.

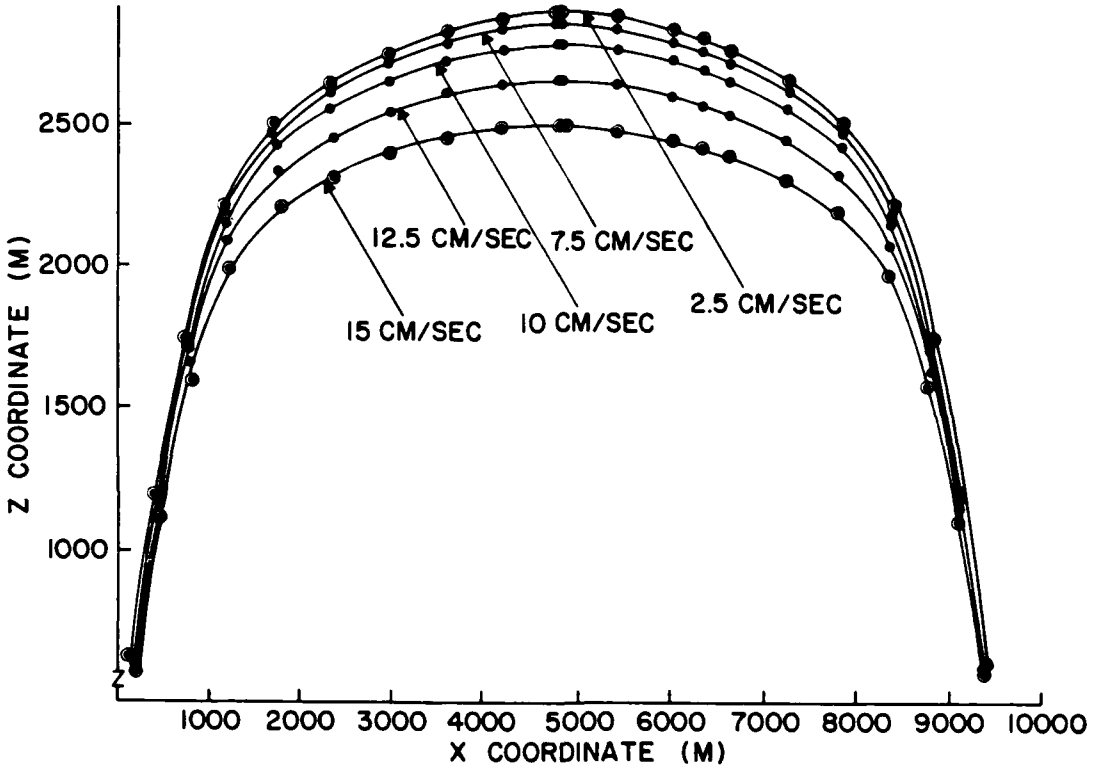

Figure 29. Side View of Cable Configuration Calculated by Static Model for Currents of 2.5, 5, 7.5, 10 cm/sec.

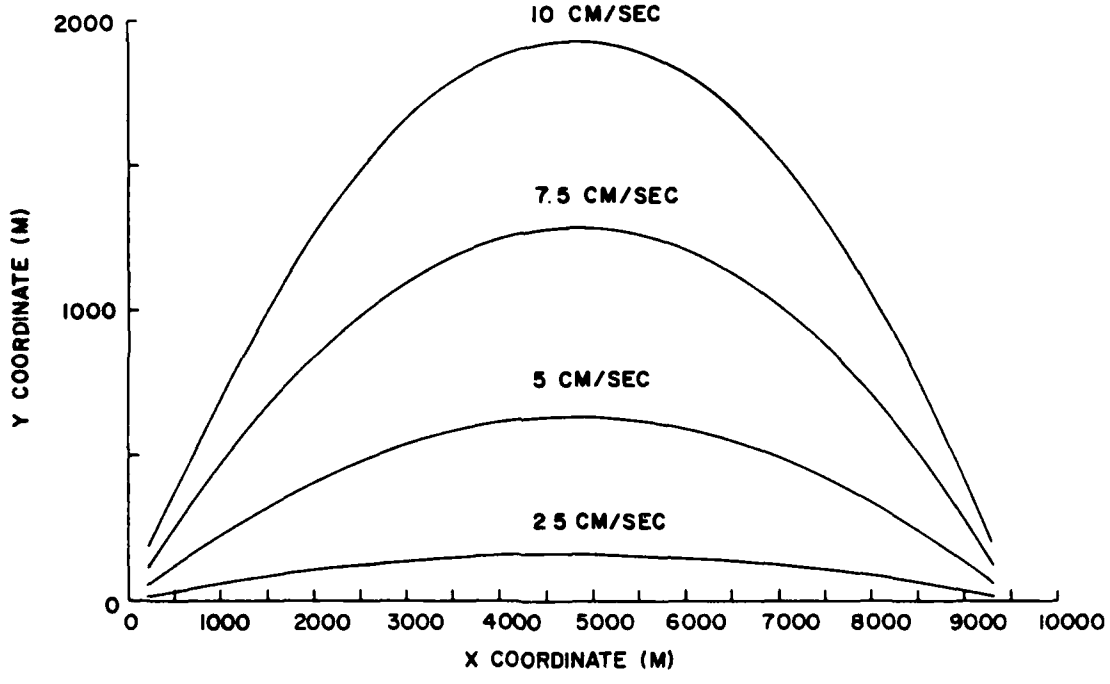

Figure 30. Static Model Output Including Strum Amplified Drag Coefficient

Table 6. Maximum Displacement of Cable for Broadside Current of 2.5 cm/sec as Function of Drag Coefficient

C_D	Maximum Displacement (m)
1.2	63
1.3	68
1.55	81
Strum Amplified C_D	157

The GRIFFIN static model used is one developed at the Naval Underwater Systems Center.[55,28] This method computes the boundary conditions by the method of imaginary reactions. The steady state differential equations are then integrated using a fourth-order Runge-Kutta method. This model features a Reynolds number dependent drag coefficient and includes the effects of tangential drag. The output of this model for several values of current is given in appendix B for comparison with other results.

A time series of static model outputs corresponding to the times of cable shape measurement in run 1 is given in figure 31. This plot was generated by putting the observed currents at each time into the GRIFFIN model and calculating the equilibrium shape of the cable. If the cable was always close to an equilibrium condition, then this time series would closely resemble the observed cable shapes during run 1 shown in figure 14. There are two things to note here. The first is that all of the model displacements are smaller than the observed

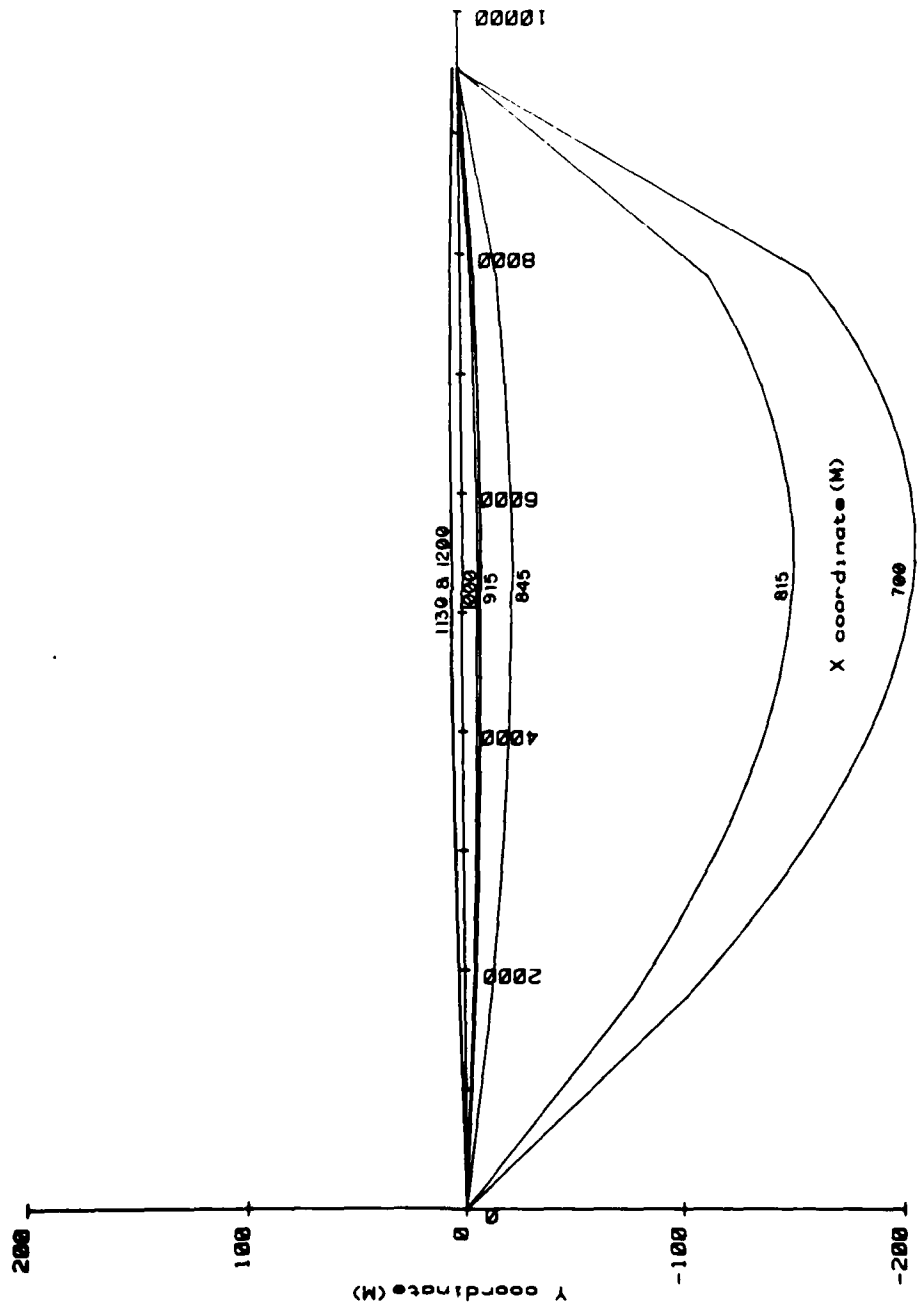

Figure 31. Time Series of Static Cable Shapes Corresponding to Run 1

displacements. This could be corrected by using a larger drag coefficient; however, the drag coefficient which would bring the model into agreement with observations at 0700 would not be the same as the drag coefficient required to accomplish the same thing at 1300. The second thing to note is that the cable observations are not in static equilibrium with the currents. The currents from 1000 to 1300 are very small and yet the cable continues to move to the extended position observed at 1311. This points up the importance of the dynamics in this problem.

4.5 Dynamic Model

The dynamic model used is one originally developed by Patton[9] and subsequently modified by Griffin.[56] It is a lumped mass model where all of the essential dynamics can be considered to be taking place at a few positions on the cable system. These positions are connected by hypothetical massless springs and damping elements. The model treats tangential and normal drag, elastic properties of the material, added mass, and damping in three dimensions.

The cable system is modeled by nine lumped mass elements as shown in figure 32. The dynamic cable equations are integrated using a fourth-order Runge-Kutta method with a time step of 0.1 sec. The effects of strumming were introduced by increasing the effective cable diameter by 25 percent. This was done based on the finding of Kennedy and Vandiver[36] that the strumming amplitudes experience a self-limiting amplitude response of about 25 percent of the cable diameter.

The dynamic response of the cable system was studied using the dynamic model. The cable was initially assumed to be at equilibrium with no current. At time t = 0 a step function change of current of

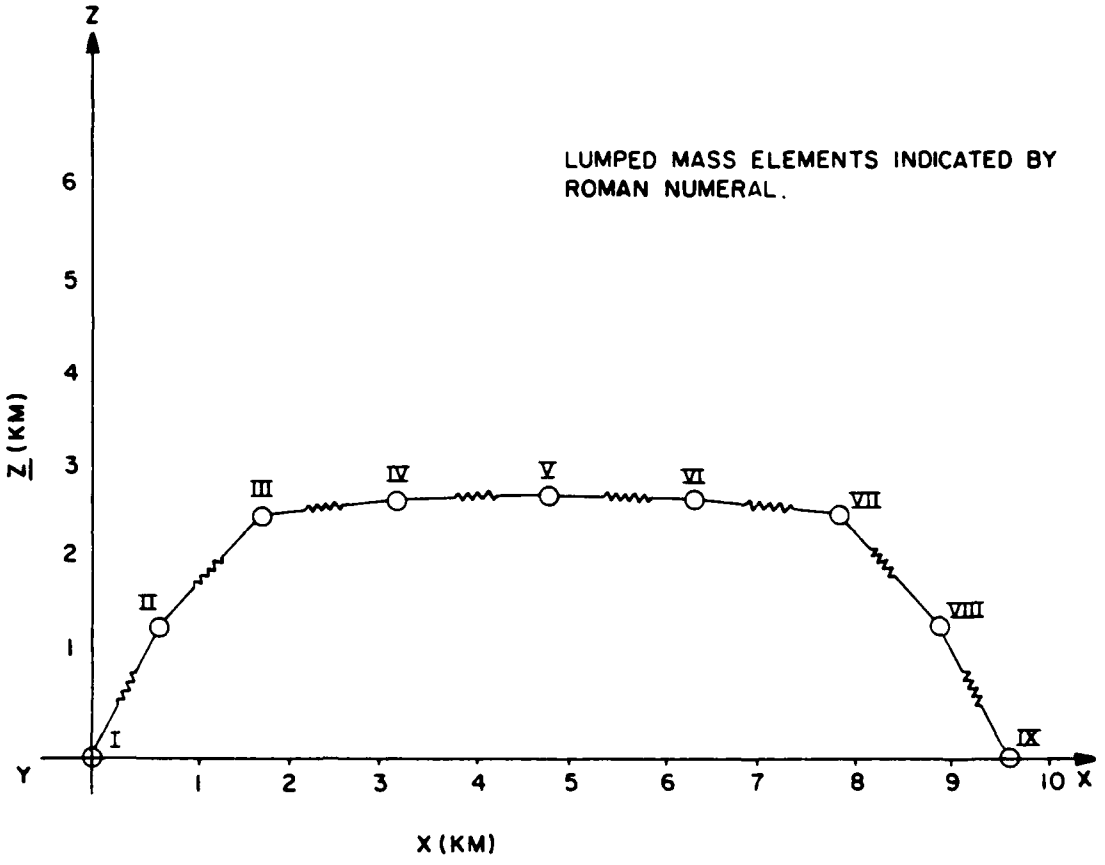

Figure 32. Schematic of Lumped Mass System

15 cm/sec broadside to the array was introduced. The computed time history of the y component of displacement for lumped mass points IV and VI are shown in figures 33 and 34. The time history curves have the appearance of the curve of a charging condenser. The equation which describes a charging condenser is

$$Y = \alpha + (y_o - \alpha)\, e^{-rt} \tag{50}$$

An equation of this form was fit to the data using a technique given by Howard, Griffin and Foye.[57] The value for r was found to be 0.0111×10^{-2} sec^{-1}. The reciprocal of r is the time constant of the charging condenser. In this case the time constant of the cable system turns out to be about 2.5 hr.

A time series of the calculated cable shape was created to correspond to the sample times of the cable shape measurements.

The model was started from a position of equilibrium with no current. The current input into the model was determined by fitting a Fourier series to the hourly averaged data. Then the current at each time step was calculated from the sum of the Fourier components. Figure 35 shows the fitted data with the original time series for the parallel and perpendicular components of the currents from EA1TOP. This is representative of the data from the other five current meters. Each of the six current meters was considered to be acting on that portion of the structure that was closest. No attempt was made to compensate for the fact that the current meters were 5 km away from the array. If changes in currents at the current measurement arrays are due to a moving disturbance (waves, advection of turbulence, frontal passage etc.) then there

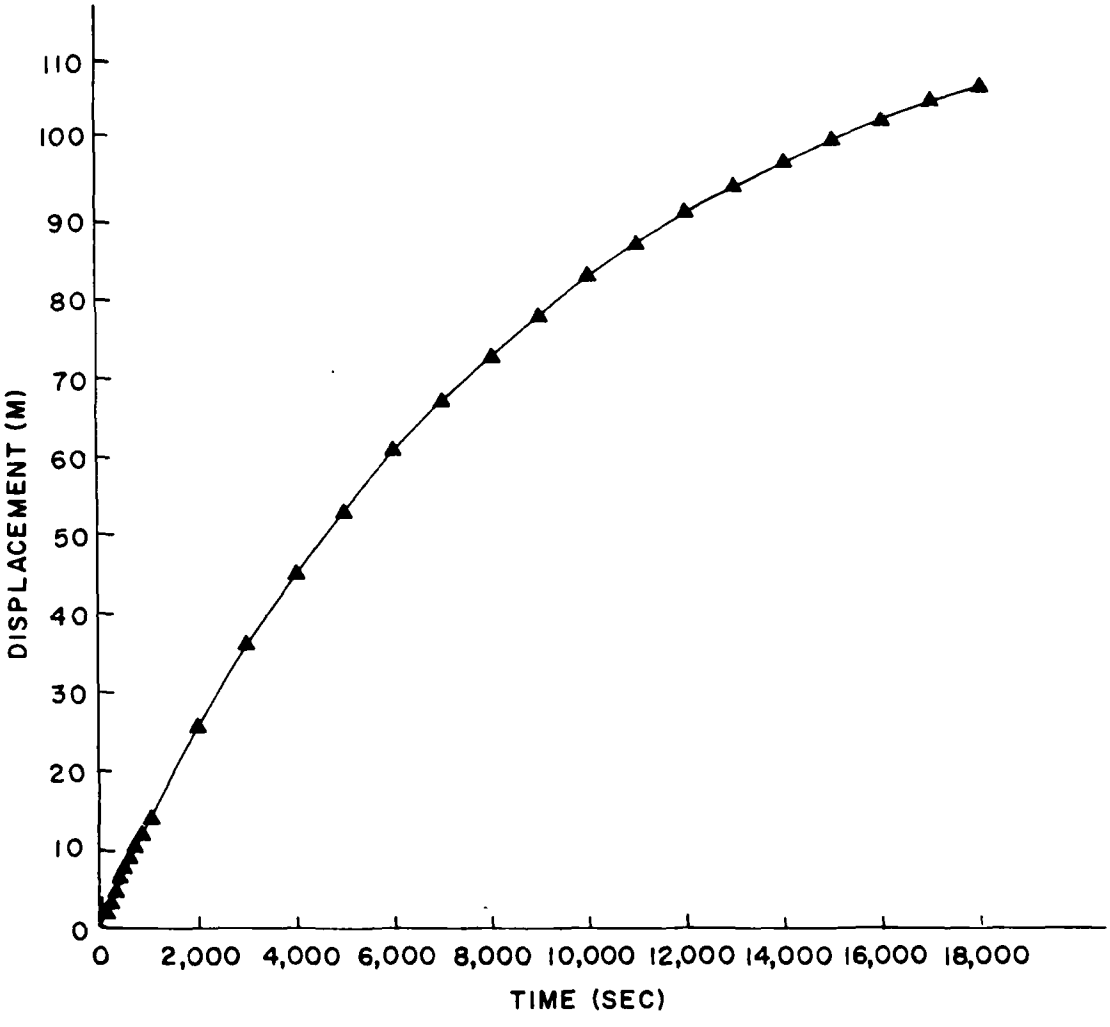

Figure 33. Time History Plot of Displacement of Lumped Mass Point IV

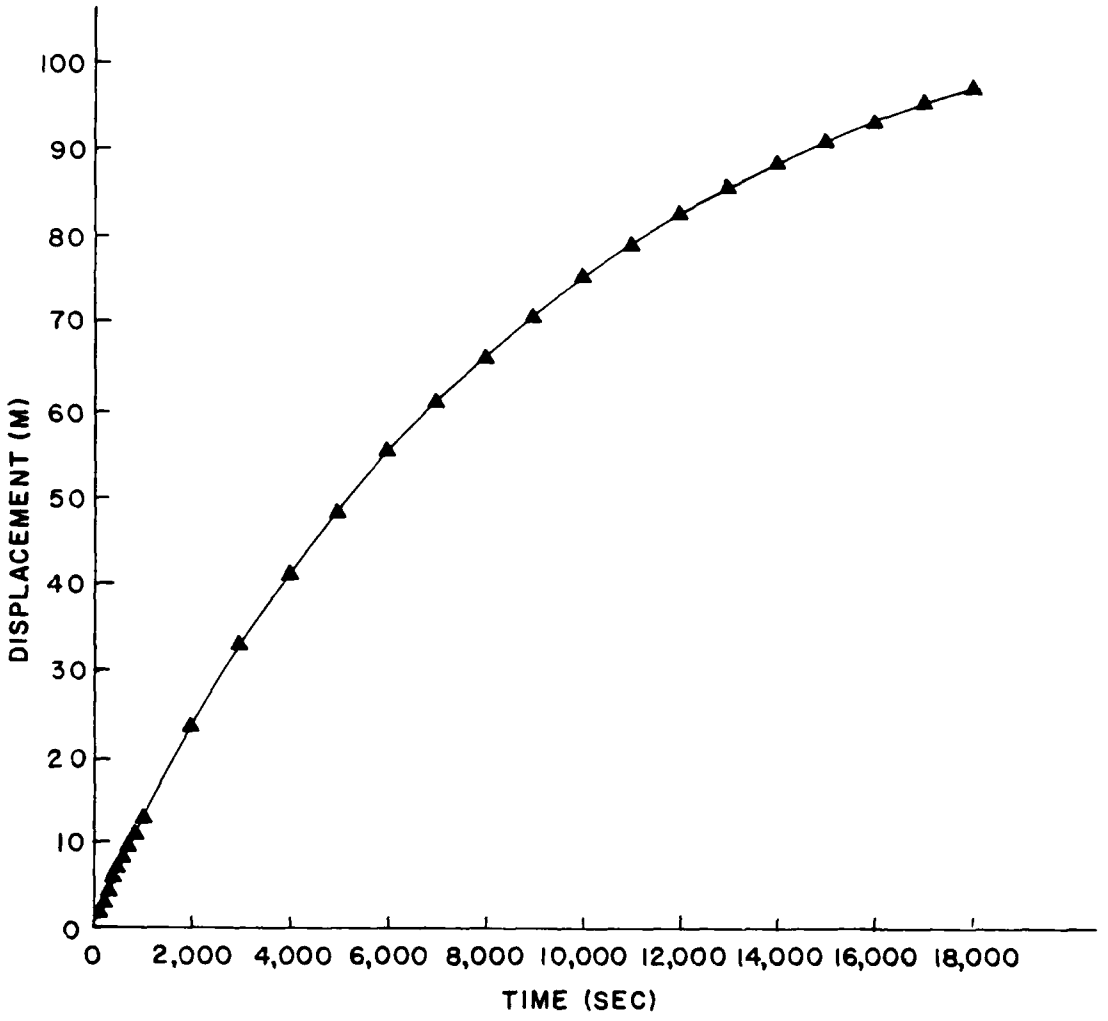

Figure 34. Time History Plot of Displacement of Lumped Mass Point VI

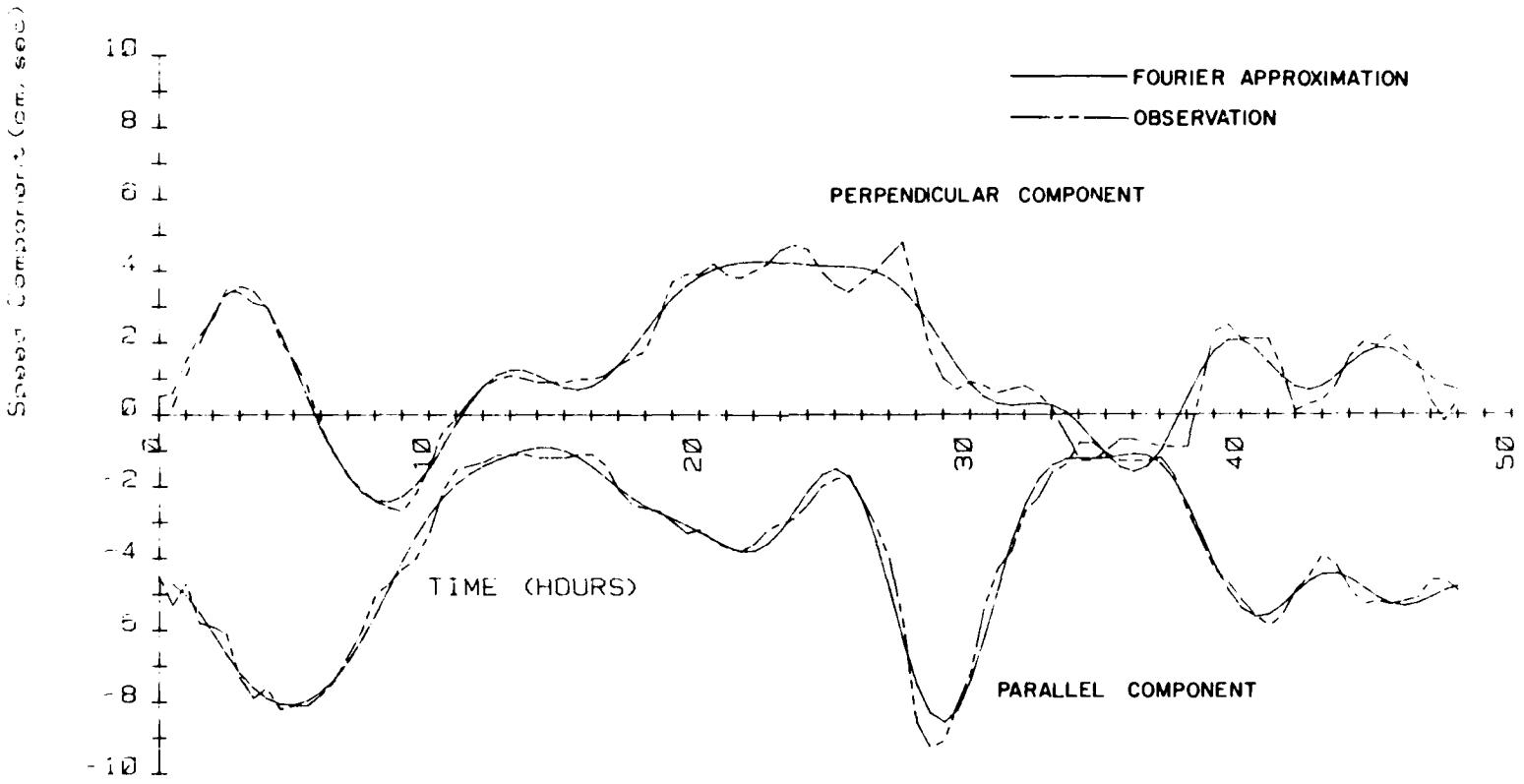

Figure 35. Current Meter Data Fitted by Fourier Series

would be a time difference between the time of an event at the measurement site and the time of the event at the cable site. When the current field is relatively homogeneous this will not be a problem. When the currents are not the same over the area, such as was the case on 27 July for example, then the currents measured at the current measurement site will not adequately describe events at the cable site.

The dynamic model was run for the currents that were measured on days 205 and 206. A limited analysis period was a result of the fact that the program requires 1 hr of computer time to calculate the array response for 1 hr of real time on the PDP 11/70 computer.

The Fourier series expansion of the current meter data is given by

$$f(t) = A_o + \sum_{n=1}^{\infty} \left[a_n \cos\left(\frac{2\pi nt}{X_B - X_A}\right) + b_n \sin\left(\frac{2\pi nt}{X_B - X_A}\right) \right] \tag{51}$$

where

$$A_o = \frac{1}{X_B - X_A} \int_{X_A}^{X_B} f(t)\, dt \tag{52}$$

$$a_n = \frac{2}{X_B - X_A} \int_{X_B}^{X_B} f(t) \cos\left(\frac{2\pi nt}{X_B - X_A}\right) dt \tag{53}$$

$$b_n = \frac{2}{X_B - X_A} \int_{X_A}^{X_B} f(t) \sin\left(\frac{2\pi nt}{X_B - X_A}\right) dt \tag{54}$$

For our case

$$X_B - X_A = 24 \text{ hours} \times 3600 \text{ sec/hr}$$

$$= 8.64 \times 10^4 \text{ sec}$$

and t is the time in seconds.

We have data from EA-1 and EA-2 at three depths on each array. The current speed was introduced in the model in the manner shown as follows.

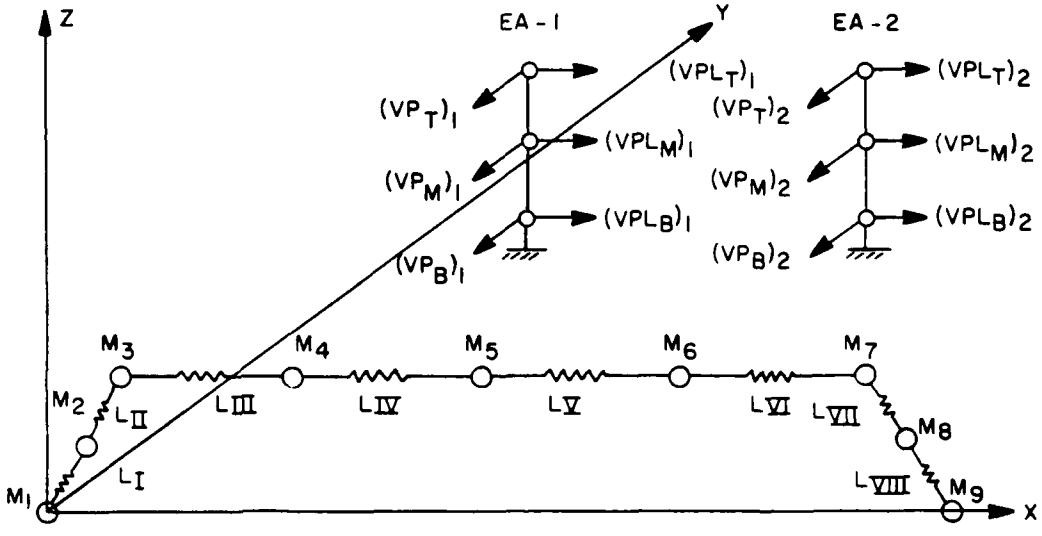

Assume that

1. $(VP_B)_1$ and $(VPL_B)_1$ act at element 1.
2. $(VP_M)_1$ and $(VPL_M)_1$ act at element 2.
3. $(VP_T)_1$ and $(VPL_T)_1$ act at element 3.
4. $(VP_T)_1$ and $(VPL_T)_1$ act at element 4.
5. $(VP_T)_2$ and $(VPL_T)_2$ act at element 5.
6. $(VP_T)_2$ and $(VPL_T)_2$ act at element 6.
7. $(VP_T)_2$ and $(VPL_T)_2$ act at element 7.
8. $(VP_B)_2$ and $(VPL_B)_2$ act at element 8.

The output of the dynamic model which corresponds to the cable shape measurements of runs 1 and 2 is given in figures 36 and 37.

4.6 Sources of Error in Modeling Effort

The principal source of uncertainty in the modeling effort comes from the fact that the current measurements were not colocated with the cable. The current meter arrays were about 5 km from the array and were separated from each other by about 4 km. The currents at each array were often different from one another and we must expect that currents at the cable location would also be different. The bulk of the horizontal span of the cable was 1 km above the highest current measurement. If there were additional current variation with depth, the input to the model could be seriously in error.

A further potential source of error comes from the fact that fundamental parameters of the array, drag coefficient and virtual mass, were

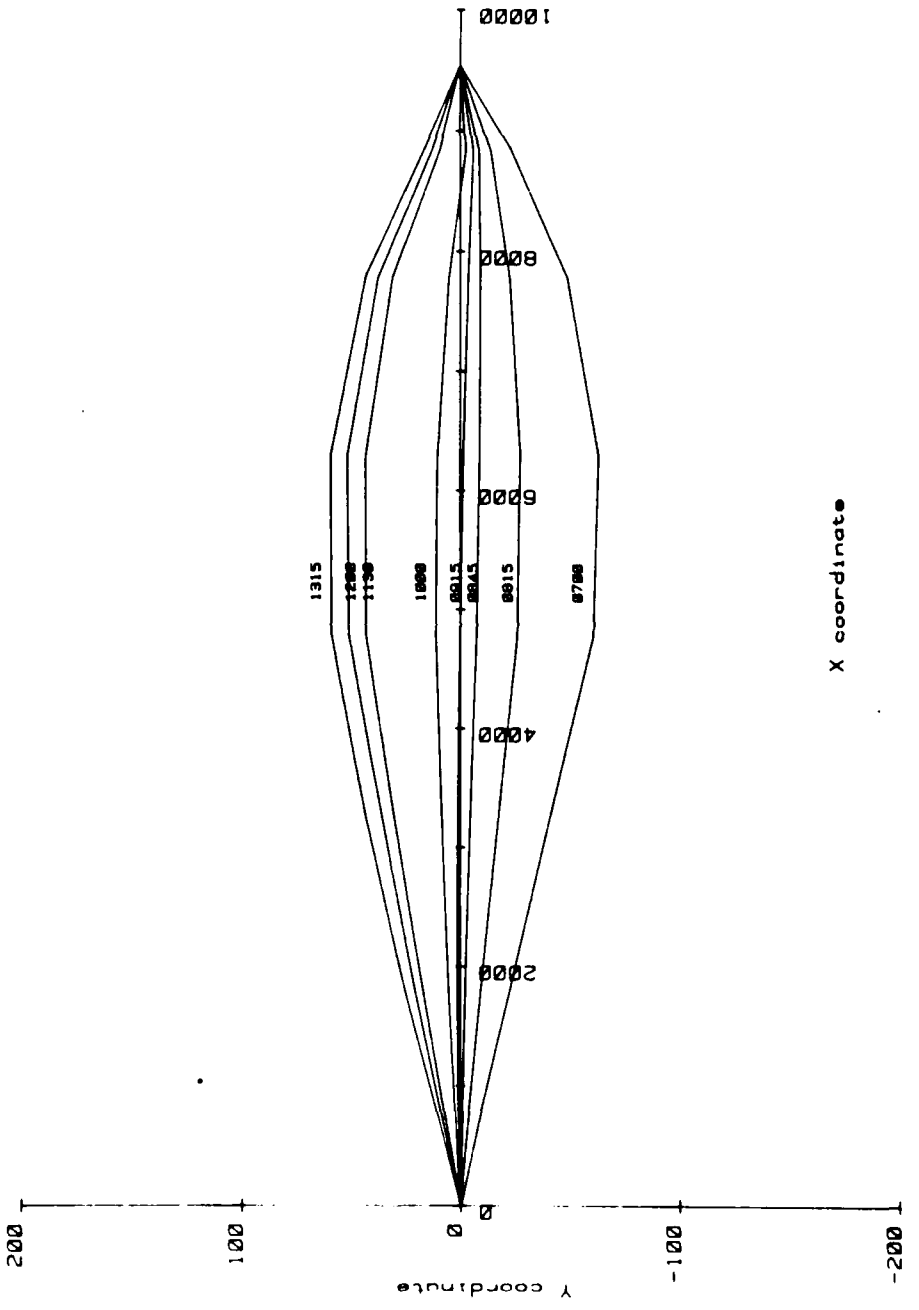

Figure 36. Output of Dynamic Model with Strumming, Run 1

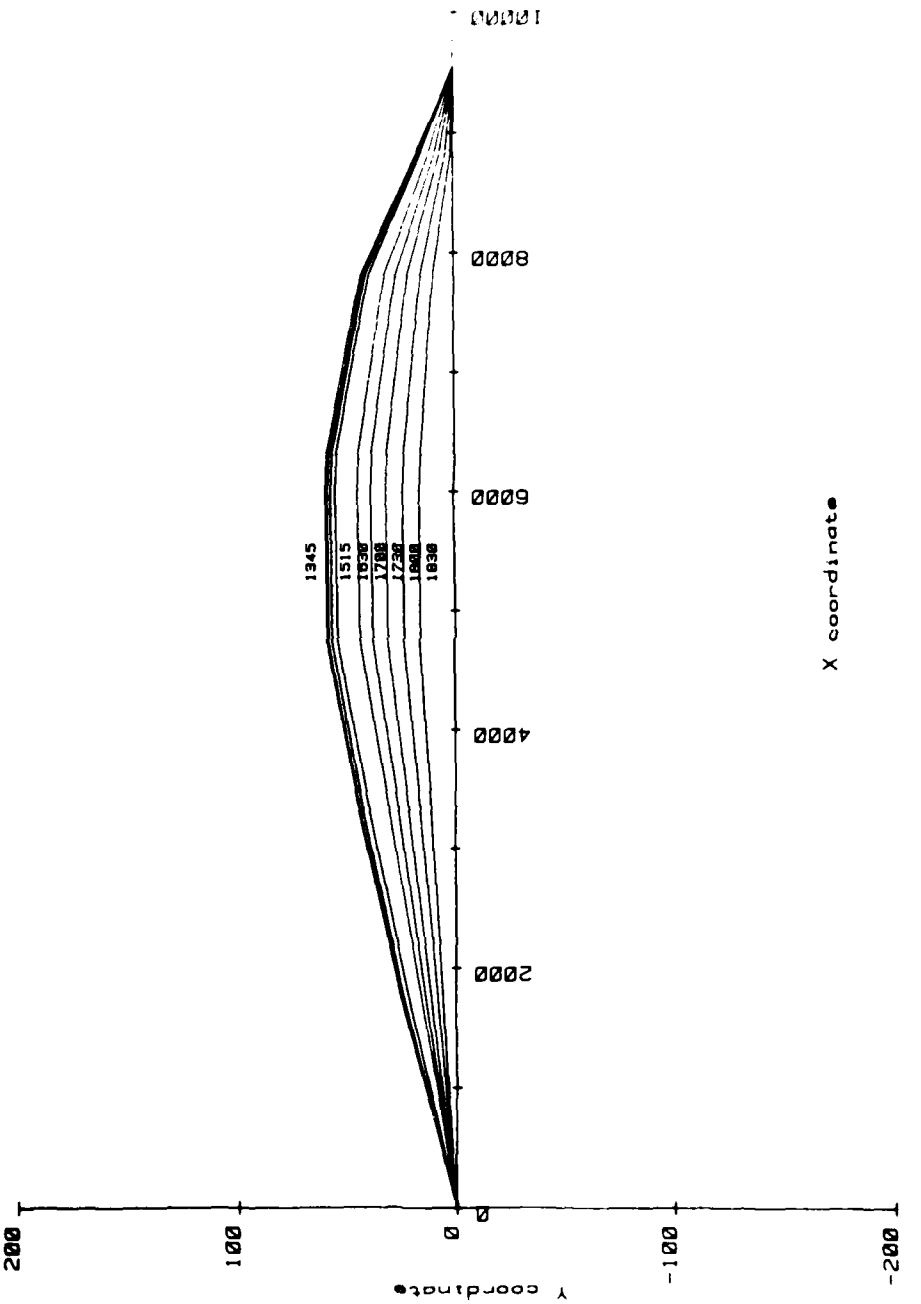

Figure 37. Output of Dynamic Model with Strumming, Run 2

not measured experimentally. The values of these parameters that were used were estimated based on results for similar cables reported in the literature. It is not known whether the cable was strumming or what the magnitude of any strumming motions might have been. Consequently any strumming effects introduced into the model are based on experience with other cables, which may or may not be applicable to this specific modeling effort.

A check on the numerical performance of the models was performed by introducing a test problem with a known solution. The simplest such problem is to consider the shape of a uniform, buoyant cable under conditions of zero current. In this case the cable shape should be a catenary. The equation of a catenary is

$$Z = c \cosh \frac{x}{c} \tag{55}$$

where c is the height of the directerix (here taken to be the x axis) and is found from

$$S = c \sinh \frac{x}{c} \tag{56}$$

for the case where the end points of the cable are at the same depth. S is the distance along the cable from the maximum height to the end of the cable and x is the coordinate of the end point. For the case where the ends of the cable are not at the same height, C is determined from

$$\sqrt{(l^2 - k^2)} = 2c \sinh \frac{h}{2c} \tag{57}$$

where h is the horizontal separation of the end points, k is the vertical separation of the end points, and l is the length of the cable. The geometry of these two cases is shown in figure 38.

The result for the static model agreed with the analytical solution to within a maximum difference of 0.4 m (table 7). The result for the case of the dynamic model was that the maximum difference was 0.2 m (table 8).

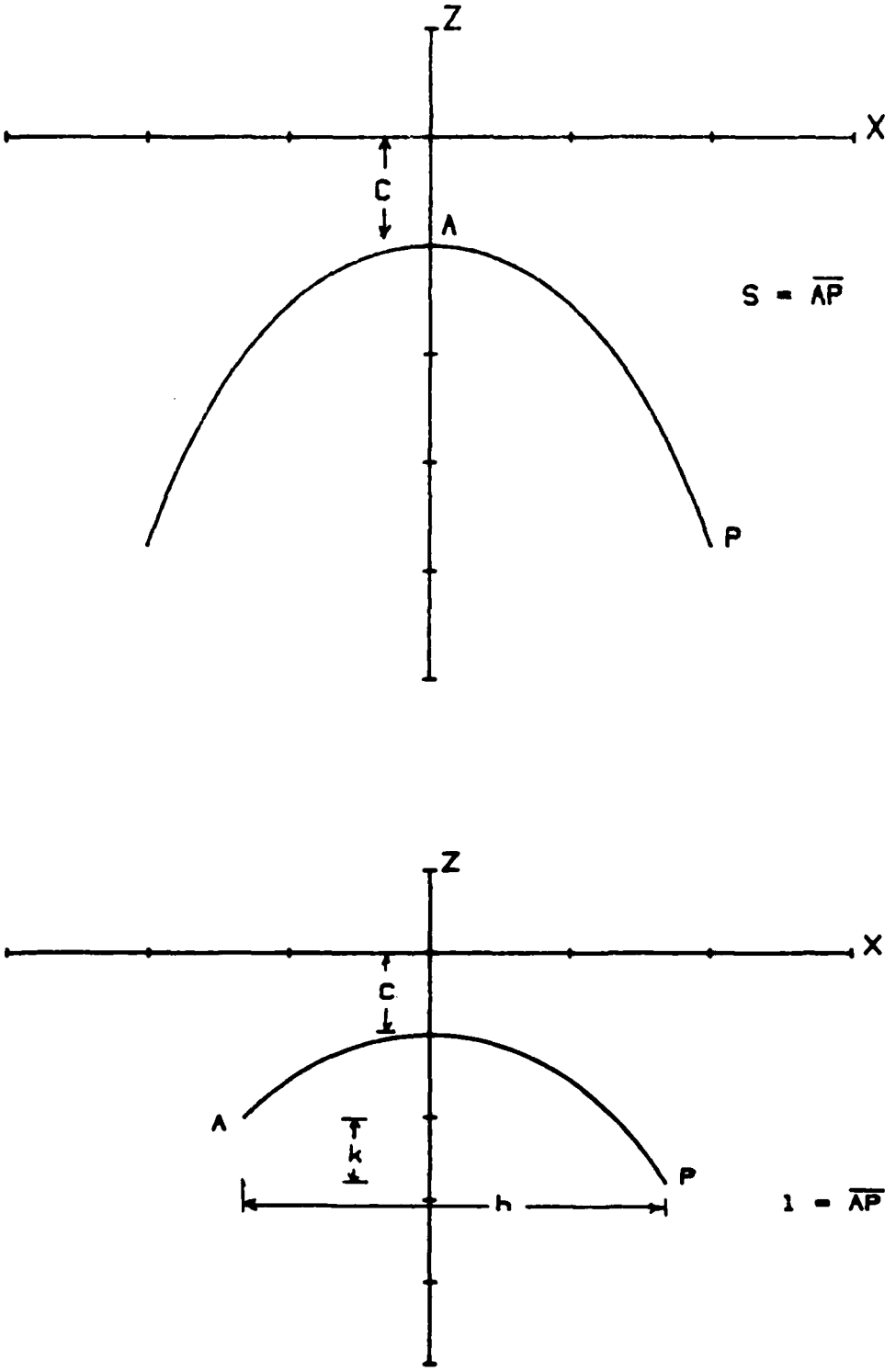

Figure 38. Schematic of Catenary Used to Test Numerical Output of Models

Table 7. Comparison of Static Model Output to Catenary for Uniform Cable, No Current

X	Z (Model)	Z (Catenary)	Difference
0.0	0.0	0.0	-0.0
334.4	515.6	515.7	-0.1
694.9	1012.9	1013.0	-0.1
1084.5	1487.0	1487.1	-0.1
1506.6	1932.1	1932.0	0.0
1964.0	2340.1	2339.9	0.2
2458.9	2701.2	2700.8	0.3
2991.3	3003.2	3002.8	0.4
3558.4	3232.9	3232.5	0.4
4152.6	3377.4	3377.0	0.4
4762.0	3426.9	3426.6	0.3
5371.3	3377.6	3377.6	0.0
5965.6	3233.4	3233.6	-0.2
6254.5	3128.0	3128.3	-0.4
6535.4	3002.7	3003.1	-0.4
7068.0	2700.8	2701.1	-0.3
7562.9	2339.8	2340.2	-0.4
8020.4	1931.9	1932.3	-0.4
8442.5	1486.9	1487.3	-0.4
8832.3	1012.8	1013.1	-0.3
9192.8	515.6	515.8	-0.2

Table 8. Comparison of Dynamic Model Output to Catenary for Uniform Cable, No Current

X	Z (Dynamic Model)	Z (Catenary)	Difference
1754.0	2567.0	2567.0	0.0
3253.7	2740.1	2739.9	0.2
4762.1	2798.6	2798.4	0.2
6270.6	2741.5	2741.3	0.2
7770.4	2569.8	2569.7	0.1

5. DISCUSSION

All of the models investigated suffer from one deficiency or another when invoked to explain this data set. There are some problems encountered in this situation that are not generally found in studies of cable deformation. For example, the length of the horizontal span (6 km) is much longer than that in any previous investigation. During much of the experiment the mean flow was directed along the cable axis. There were times when there were significant shears in both the vertical and in the horizontal current field.

It is still an open question as to whether the cables were strumming or not. If the cables were strumming then the effective drag coefficient should be increased, an effect that would improve the agreement between the models and the observations because all of the models underestimate the cable displacement. However, when the strum amplified drag coefficient proposed by Skop and Rosenthal[34] is used (figure 30), the model maximum displacements are larger than observed displacements by a factor of about 2. This discrepancy could be due to the fact that the Skop and Rosenthal expression was derived from empirical results obtained from the wake response of rigid cylinders. There is some indication in the work of Kennedy and Vandiver[36] that the strumming characteristics of rigid cylinders are different from flexible cables. A more conservative strum amplification was used in the dynamic model with the result that the model underestimated the observed deflections by a factor of about 2.

It is possible to force agreement of the model results and observation by selection of the drag coefficient which would lead to the best fit of the data. We find, however, that no single drag coefficient is adequate to explain all of the data.

When a time series formed from the static model results is compared to observations from run 1, it is found that quantitatively there is an initial agreement, but as time goes on the agreement with the observations becomes less and less. Particularly after about 1000, the observed cable deflection was to bow out on the north side of the x axis. The static model results are that the cable remains close to the x axis. It is interesting that the dynamic model does track the observations through this period fairly well. This illustrates the importance of the dynamics in the cable behavior problem.

Another possible reason for the difference in results between models and observations is related to computational methodology. The intent of this study was to take several models as they stand and see how well they explained the observations. A check was performed against a problem with a known analytical solution and the agreement was good. Even so, it is still possible that hitherto undetermined numerical problems remain in some of the models. For example, Meggit reported that a dynamic model he was investigating turned out to be sensitive to the initially assigned cable shape.[8]

6. CONCLUSIONS

The development of cable models has proceeded without the checks and balances of interaction with experiment. We have shown the importance of dynamics in the prediction of cable configuration. The dynamic model predicted the qualitative behavior of the cable through a complete current cycle. Quantitatively, however, the dynamic model predicted displacements about half as large as observed.

Agreement between model results and observation can be improved by introducing in some way the effects of strumming. One suggested way to improve the agreement is to increase the effective cable diameter by the strumming amplitude. This was done with the dynamic model to obtain the result stated above. Another proposed method is to increase the drag coefficient by a strum amplification factor which is a function of the Reynolds number. When this was done with the present data set the model results overestimated the observed results by a factor of 2. The modeling of strumming effects is still an open issue.

None of the model outputs investigated corresponded exactly with the observations. There are a number of adjustable parameters in the models that can be used to force agreement. A better approach would be to make direct measurements of as many of these parameters as possible and remove these sources of uncertainties from the problem. Accelerometers should be included in the measurements made on the cable. Laboratory tests should be made to determine material properties, drag coefficients, and added mass coefficients.

AD-A099 781 NAVAL UNDERWATER SYSTEMS CENTER NEW LONDON CT NEW LO--ETC F/G 13/13
DYNAMICS OF UNDERSEA CABLES,(U)
MAY 81 J M SYCK
UNCLASSIFIED NUSC-TR-6313 NL

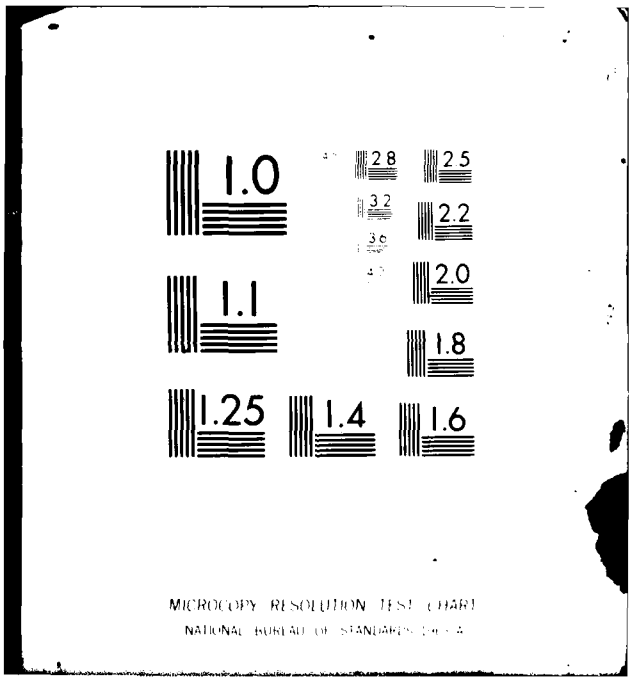
1.0
2.8
2.5
3.2
2.2
3.6
2.0
1.1
1.8
1.25
1.4
1.6
MICROCOPY RESOLUTION TEST CHART
NATIONAL BUREAU OF STANDARDS

The dynamic model results show that the array moves so slowly that it never reaches the "static equilibrium" condition. It is tempting to try to recreate the time history of array displacement by successive calculations of the equilibrium configuration, but it is clear that this will not work. The value in calculating the equilibrium configuration is that it provides engineering design numbers. It cannot provide insight into the behavior of a cable system subject to ocean current forcing.

It is the low frequency components of the flow that dominate the array motion. This is shown by the fact that the spectrum of the array motion is dominated by a peak at the tidal frequency.

REFERENCES

1. N. D. Albertson, A Survey of Techniques for the Analysis and Design of Submerged Mooring Systems, NCEL TR R815, Naval Civil Engineering Laboratory, Port Hueneme, CA, August 1974.
2. Sir Horrace Lamb, Statics, Cambridge University Press, London, England, 1924.
3. L.I. Davis, E. M. Fitzgerald, and J. J. Neilligan, Bibliography on Deep Sea Mooring Technology, Hydrospace Research Corporation Report 110, November 1963.
4. M. J. Casarella and M. Parsons, "Cable Systems Under Hydrodynamic Loading," Marine Technology Society Journal, Vol. 4, 1970, pp. 27-44.
5. R. King, "A Review of Vortex Shedding Research and Its Application," Ocean Engineering, Vol. 5, 1977, pp. 141-147.
6. E. F. Buck and D. J. Meggitt, "Laboratory Experiments on the Large Displacement Dynamics of Cable Systems," Civil Engineering Laboratory, Naval Construction Battalion Center, Port Hueneme, CA, Technical Memorandum No. 44-78-06, February, 1978.
7. B. J. Noonan, M. J. Casarella, and Y Choo, "An Experimental Study of the Motion of a Towline Attached to a Vehicle Moving in a Circular Path," 8th Annual Conference of Marine Technology Society, 1972, pp. 97-116.
8. D. J. Meggitt and D. B. Dillon, "At Sea Measurements of the Dynamic Response of a Single Point Mooring During Deployment," Civil Engineering Laboratory, Naval Construction Battalion Center, Port Hueneme, CA, Technical Memorandum No. 44-78-09, March 1978.

9. K. T. Patton, "The Response of Cable-Moored Axisymmetric Buoys to Ocean Wave Excitation," PhD Dissertation, University of Rhode Island, June 1972.

10. B. A. Wilson, Characteristics of Anchor Cables in Uniform Ocean Currents, OTR 204-1, Texas A&M University, College Station, TX, April 1960.

11. R. O. Reid, Dynamics of Deep-Sea Mooring Lines, Project 204, Ref 68-11F, Texas A&M University, College Station, TX, July 1968.

12. J. W. Bedenbender, "Three Dimensional Boundary Value Problems for Flexible Cables," OTC 1281 in Proceedings 2nd Annual Offshore Technology Conference, Houston, TX, 1970.

13. A. P. K. DeZoysa, "Steady-State Analysis of Underseas Cables," Ocean Engineering, Vol. 5, No. 3, pp. 209-229, January 1978.

14. R. A. Skop and G. J. O'Hara, The Static Equilibrium Configuration of Cable Arrays by Use of the Method of Imaginary Reactions, NRL Report 6819, Naval Research Laboratory, Washington, D.C., February 1969.

15. R. A. Skop and J. Mark, A Fortran IV Program for Computing the Static Deflections of Structural Cable Arrays, NRL Report 7640, Naval Research Laboratory, Washington, D.C., August 1973.

16. R. Paquette and B. E. Henderson, Dynamics of Simple Deep Sea Buoy Moorings, General Motors Defense Research Laboratory Technical Report 65-79, 1965.

17. B. J. Morgan, "The Finite Element Method and Cable Dynamics," Proceedings of Symposium on Ocean Engineering, University of Pennsylvania, Philadelphia, PA, 1970.

18. R. L. Webster "Finite Element Analysis of Deep-Sea Moors and Cable Systems," ASCE Fall Convention Preprint 3033, San Francisco, CA, October 17-21, 1977.

19. C. Holm and H. A. DeFerrari, "Ocean Engineering," in Handbook of Marine Science, Vol. 1, CRC Press, Cleveland, OH, 1974.

20. H. O. Berteaux, Buoy Engineering, John Wiley and Sons, New York, NY, 1976.

21. O. M. Griffin, J. H. Pattison, R. A. Skop, S. E. Ramberg, and D. J. Meggitt, "Vortex Excited Vibrations of Marine Cables," ASCE Journal of Waterways, Port; Coastal and Ocean Divisions, May 1980.

22. J. B. Keller, "Large Amplitude Motion of a String," American Journal of Physics, Vol. 27, 1959, p. 584.

23. N. Cristescu, "Spatial Motion of Elastic-Plastic Strings," Journal of Mechanical Physical Solids, Vol. 9, 1961, pp. 165-178.

24. N. Cristescu, "Rapid Motions of Extensible Strings," Journal of Mechanical Physical Solids, Vol. 12, pp. 269-278, 1964.

25. G. E. Forsythe and W. R. Wasow, Finite-Difference Methods for Partial Differential Equations, John Wiley and Sons, New York, NY, 1960.

26. Y. Choo and M. J. Casarella, A Survey of Analytical Methods for Dynamic Simulation of Cable-Body Systems, Catholic University, Department of Civil and Mechanical Engineering Report 73-1, March 1973.

27. S. C. Daubin, Sensitivity Analysis of Inclinometer Line Current Profiling System, Technical Report UM-RSMAS-73074, University of Miami, 1973.

28. J. P. Radochia, A Steady State and Dynamic Analysis of a Mooring System, NUSC Technical Report 5597, Naval Underwater Systems Center, New London, CT, 25 March 1977.

29. R. A. Skop and G. J. O'Hara, Analysis of Internally Redundant Structural Cable Arrays, NRL Report 7296, Naval Research Laboratory, Washington, D.C., September 1971.

30. M. C. Eames, "Steady-State Theory of Towing Cables," Trans. R. Instn. Nav. Archit., Vol 110, pp. 185-206, 1968.

31. T. R. Kretschmer, G. A. Edgerton, and N. P. Albertsen, Sea Floor Construction Experiment, SEACON II: An Instrumented Tri-Moor for Evaluating Undersea Cable Structure Technology, Civil Engineering Laboratory Technical Report R848, December 1976.

32. H. U. Sverdrup, M. W. Johnson, and R. H. Fleming, The Oceans, Prentice Hall, Englewood Cliffs, NJ, 1942.

33. J. D. Wilcox, "A Summary of Tangential Drag Formulations for Cables," NUSC Technical Memorandum No. SA23-398-73, Naval Underwater Systems Center, New London, CT, August 1973.

34. R. A. Skop and F. Rosenthal, "Some New Approximation Techniques for Mooring System Design," Marine Technology Society Journal, Vol. 13, No. 6, pp. 9-13, 1980.

35. B. LeMehaute, An Introduction to Hydrodynamics and Water Waves, Springer Verlag, New York, NY, 1976.

36. M. Kennedy and J. K. Vandiver, "A Random Vibration Model For Cable Strumming Prediction," Proceedings of ASCE: Civil Engineering in the Ocean, IV, San Francisco, CA, 10 September 1979.

37. T. Sarpkaya, "Vortex Induced Oscillations," Journal of Applied Mechanics, Vol. 46, pp. 241-258, 1979.

38. J. R. Dale and J. M. McCandless, Water Drag Effects of Flow Induced Cable Vibrations, Naval Air Development Center, Warminster, PA, Report NADC-AE-6731, September 1967.

39. Sir Horrace Lamb, Hydrodynamics, Dover Press, New York, NY, 1945.

40. K. T. Patton, "Tables of Hydrodynamics MASS Factors for Translational Motion," ASME Annual Conference, Winter 1965.

41. S. E. Ramberg and O. M. Griffin, Some Transverse Resonant Vibration Characteristics of Wire Rope, with Application to Flow-Induced Cable Vibrations, Navy Research Laboratory Report 7821, December 1974.

42. J. H. Pattison, P. P. Rispin, and N. T. Tsai, Handbook on Hydrodynamic Characteristics of Moored Array Components, David Taylor Naval Ship Research and Development Center, March 1977.

43. R. R. Miller, "The Effects of Frequency and Amplitude of Oscillation on the Hydrodynamic Mass of Irregular Shaped Bodies," M.S. Thesis, University of Rhode Island, 1965.

44. R. R. Miller and W. M. Hagist, Experimental Determination of Hydrodynamic Mass, University of Rhode Island Division of Engineering Research and Development, Report to U. S. Navy Underwater Sound Laboratory, Kingston, RI, 1965.

45. S. E. Ramberg and O. M. Griffin, Some Transverse Resonant Vibration Characteristics of Wire Rope, With Application to Flow Induced Cable Vibrations, NRL Technical Report 7821, Naval Research Laboratory, Washington, D.C., December 1974.

46. A. C. Callahan, OMAT Alternative Active Array Shape Algorithm Description, Raytheon Company, Portsmouth, RI, 3 December 1979.

47. R. M. Hendry and A. J. Hartling, "A Pressure-Induced Direction Error in Nickel-Coated Aanderaa Current Meters," Deep-Sea Research, Vol. 26, pp. 327-336, 1979.

48. C. DeBoor, "Bicubic Spline Interpolation," Journal of Math and Physics, Vol. 41, pp. 212-218, 1962.

49. A. H. Nuttall, Spectral Analysis of a Univariate Process with Bad Data Points, Via Maximum Entropy and Linear Predictive Techniques, NUSC Technical Report No. 5303, Naval Underwater Systems Center, New London, CT, 26 March 1976.

50. H. Weinberg, Generic Sonar Model, NUSC Technical Document 5971A, Naval Underwater Systems Center, New London, CT, 27 February 1980.

51. L. V. Worthington, "On the North Atlantic Circulation," The Johns Hopkins Oceanographic Studies No. 6, The Johns Hopkins University Press, Baltimore, MD, 1976.

52. W. B. Owens and N. G. Hogg, "Oceanic Observations of Stratified Taylor Columns Near a Bump," Deep-Sea Res., Vol. 27, No. 12A, pp. 1029-1046, December 1980.

53. S. Sergev, DECEL1 Users Manual - A FORTRAN IV Program for Computing the Static Deflections of Structural Cable Arrays, Technical Note 1584, Naval Construction Battalion Center, Port Hueneme, CA, August 1980.

54. J. S. Patel, "DESADE Data Generation Program for Cable Network in Variable Velocity Current Profile," NUSC Technical Memorandum TM-EM-41-75, Naval Underwater Systems Center, New London, CT, 15 December 1975.

55. Personal communication with G. T. Griffin and G. R. Swope, 1976.

56. G. T. Griffin, Dynamics of a Cable-Towed-Body System, NUSC Technical Report 4709, Naval Underwater Systems Center, New London, CT, 10 July 1974.

57. B. E. Howard, G. T. Griffin, and M. P. Foye, "Curve Fitting Acoustical Data," submitted for publication, 1981.

APPENDIX A

JULIAN DATE CALENDAR

(PERPETUAL)

DAY	JAN	FEB	MAR	APR	MAY	JUN	JULY	AUG	SEP	OCT	NOV	DEC	DAY
1	001	032	060	091	121	152	182	213	244	274	305	335	1
2	002	033	061	092	122	153	183	214	245	275	306	336	2
3	003	034	062	093	123	154	184	215	246	276	307	337	3
4	004	035	063	094	124	155	185	216	247	277	308	338	4
5	005	036	064	095	125	156	186	217	248	278	309	339	5
6	006	037	065	096	126	157	187	218	249	279	310	340	6
7	007	038	066	097	127	158	188	219	250	280	311	341	7
8	008	039	067	098	128	159	189	220	251	281	312	342	8
9	009	040	068	099	129	160	190	221	252	282	313	343	9
10	010	041	069	100	130	161	191	222	253	283	314	344	10
11	011	042	070	101	131	162	192	223	254	284	315	345	11
12	012	043	071	102	132	163	193	224	255	285	316	346	12
13	013	044	072	103	133	164	194	225	256	286	317	347	13
14	014	045	073	104	134	165	195	226	257	287	318	348	14
15	015	046	074	105	135	166	196	227	258	288	319	349	15
16	016	047	075	106	136	167	197	228	259	289	320	350	16
17	017	048	076	107	137	168	198	229	260	290	321	351	17
18	018	049	077	108	138	169	199	230	261	291	322	352	18
19	019	050	078	109	139	170	200	231	262	292	323	353	19
20	020	051	079	110	140	171	201	232	263	293	324	354	20
21	021	052	080	111	141	172	202	233	264	294	325	355	21
22	022	053	081	112	142	173	203	234	265	295	326	356	22
23	023	054	082	113	143	174	204	235	266	296	327	357	23
24	024	055	083	114	144	175	205	236	267	297	328	358	24
25	025	056	084	115	145	176	206	237	268	298	329	359	25
26	026	057	085	116	146	177	207	238	269	299	330	360	26
27	027	058	086	117	147	178	208	239	270	300	331	361	27
28	028	059	087	118	148	179	209	240	271	301	332	362	28
29	029		088	119	149	180	210	241	272	302	333	363	29
30	030		089	120	150	181	211	242	273	303	334	364	30
31	031		090		151		212	243		304		365	31

FOR LEAP YEAR ADD ONE TO DATES AFTER 28 FEBRUARY

APPENDIX B - MODEL OUTPUT AS A FUNCTION OF CURRENT SPEED

MODEL NAME DESADE

DRAG COEFFICIENT 1.2

CURRENT SPEED 2.5 CM/SEC

X-COORD (M)	Y-COORD (M)	Z-COORD (M)
201.46	6.34	604.57
445.84	13.17	1187.47
754.22	20.66	1733.01
1160.68	29.14	2201.74
1697.68	38.43	2493.90
2300.27	46.97	2632.92
2908.90	53.73	2742.21
3522.16	58.70	2821.06
4138.56	61.84	2868.85
4756.60	63.12	2885.19
5374.67	62.51	2870.01
5991.16	60.04	2823.38
6302.74	58.09	2787.87
6613.35	55.65	2744.56
7222.16	49.53	2636.36
7825.02	41.60	2498.42
8363.06	32.49	2206.64
8770.56	23.59	1737.49
9079.85	15.30	1190.92
9325.05	7.41	606.52

MODEL NAME DESADE

DRAG COEFFICIENT 1.2

CURRENT SPEED 5.0 CM/SEC

X-COORD (M)	Y-COORD (M)	Z-COORD (M)
201.86	25.33	603.96
446.66	52.51	1186.07
755.50	82.44	1730.60
1162.27	116.09	2197.96
1698.93	153.06	2488.75
2300.88	186.99	2626.85
2909.11	213.90	2735.51
3522.19	233.68	2813.84
4138.56	246.14	2861.32
4756.60	251.20	2877.54
5374.70	248.80	2862.39
5991.22	239.01	2815.97
6302.77	231.24	2780.65
6613.32	221.58	2737.55
7221.82	197.17	2629.93
7824.14	165.74	2492.81
8361.87	129.50	2202.38
8769.61	94.06	1734.65
9079.24	60.96	1189.21
9324.78	29.81	605.73

MODEL NAME DESHDE

DRAG COEFFICIENT 1.2

CURRENT SPEED 7.5 CM/SEC

X-COORD (M)	Y-COORD (M)	Z-COORD (M)
203.41	56.32	601.34
450.02	116.76	1180.25
760.74	183.08	1720.54
1168.73	257.39	2182.26
1703.99	338.56	2467.39
2303.32	412.83	2601.92
2909.97	471.93	2707.77
3522.25	515.36	2784.15
4138.40	542.76	2830.39
4756.60	553.92	2846.08
5374.89	548.67	2831.12
5991.34	527.16	2785.58
6302.80	510.06	2750.99
6613.11	488.88	2708.81
7220.36	435.29	2603.60
7820.45	366.44	2469.70
8356.93	286.86	2184.79
8765.62	208.66	1722.92
9076.74	135.39	1182.17
9323.62	66.23	602.47

MODEL NAME DESHDE

DRAG COEFFICIENT 1.2

CURRENT SPEED 10.0 CM/SEC

X-COORD (M)	Y-COORD (M)	Z-COORD (M)
207.13	97.41	594.85
458.00	201.58	1165.74
773.13	315.33	1695.70
1183.82	441.66	2143.95
1715.82	577.72	2416.00
2309.17	701.65	2542.37
2912.10	800.67	2641.94
3522.58	873.70	2713.81
4138.31	919.90	2757.21
4756.78	938.71	2771.72
5375.50	929.96	2757.15
5991.89	893.72	2713.65
6303.17	864.98	2680.68
6612.89	829.32	2640.54
7217.25	739.47	2540.78
7812.34	624.44	2414.20
8345.84	491.04	2141.94
8756.54	358.31	1694.06
9071.01	232.98	1164.74
9321.03	114.14	594.39

MODEL NAME DECEL1

DRAG COEFFICIENT 1.3

CURRENT SPEED 2.5 CM/SEC

X-COORD (M)	Y-COORD (M)	Z-COORD (M)
250.73	8.65	752.53
591.80	18.20	1466.17
1049.62	29.08	2095.98
2456.02	52.73	2665.32
3219.32	60.93	2787.08
3988.69	66.08	2860.96
4761.14	68.09	2886.07
5533.62	66.93	2862.18
6303.08	62.66	2789.48
7066.60	55.32	2668.91
8474.55	32.67	2100.94
8935.69	20.94	1470.25
9267.60	10.15	754.89

MODEL NAME DECEL1

DRAG COEFFICIENT 1.3

CURRENT SPEED 5.0 CM/SEC

X-COORD (M)	Y-COORD (M)	Z-COORD (M)
259.28	34.50	751.60
593.05	72.48	1464.00
1051.42	115.88	2092.05
2456.57	209.75	2658.03
3219.48	242.37	2778.91
3988.66	262.79	2852.24
4761.17	270.77	2877.17
5533.71	266.26	2853.34
6303.11	249.28	2781.10
7066.26	220.12	2661.26
8473.15	130.08	2096.46
8932.58	83.45	1467.66
9267.21	40.48	753.76

MODEL NAME DECEL1

DRAG COEFFICIENT 1.3

CURRENT SPEED 7.5 CM/SEC

X-COORD (M)	Y-COORD (M)	Z-COORD (M)
261.63	76.59	747.70
598.05	160.71	1454.95
1058.76	256.45	2075.59
2458.98	461.63	2628.13
3220.02	532.95	2745.50
3988.69	577.69	2816.67
4761.32	595.21	2840.72
5534.07	585.34	2817.28
6303.20	548.19	2746.69
7064.98	484.33	2629.87
8467.57	287.53	2077.81
8917.86	184.79	1456.87
9265.50	89.73	748.92

MODEL NAME DECEL1

DRAG COEFFICIENT 1.3

CURRENT SPEED 10.0 CM/SEC

X-COORD (M)	Y-COORD (M)	Z-COORD (M)
267.05	131.91	738.10
609.75	276.07	1432.76
1075.65	438.56	2035.81
2464.49	779.52	2558.15
3221.46	898.26	2667.72
3988.84	973.06	2734.11
4761.84	1002.50	2756.17
5535.20	985.98	2733.59
6303.66	923.90	2666.66
7062.36	817.53	2556.45
8455.07	490.22	2032.98
8920.30	316.25	1430.66
9261.66	153.92	737.12

MODEL NAME DESADE

DRAG COEFFICIENT 1.55

CURRENT SPEED 2.5 CM/SEC

X-COORD (M)	Y-COORD (M)	Z-COORD (M)
201.49	8.20	604.54
448.87	17.01	1187.41
754.28	26.70	1732.89
1160.77	37.61	2201.55
1697.74	49.62	2493.66
2300.34	60.65	2632.61
2908.93	69.40	2741.88
3522.19	75.80	2820.69
4138.59	79.85	2868.45
4756.63	81.50	2884.82
5374.70	80.71	2869.61
5991.19	77.54	2822.98
6302.77	75.01	2787.50
6613.38	71.87	2744.19
7222.19	63.94	2636.00
7825.02	53.73	2498.11
8363.03	41.97	2206.40
8770.56	30.45	1737.31
9079.85	19.72	1190.80
9325.08	9.63	606.43

MODEL NAME DESADE

DRAG COEFFICIENT 1.55

CURRENT SPEED 5.0 CM/SEC

X-COORD (M)	Y-COORD (M)	Z-COORD (M)
202.13	32.64	603.54
447.24	67.69	1185.10
756.42	106.25	1728.89
1163.40	149.59	2195.31
1699.82	197.14	2485.13
2301.34	240.72	2622.62
2909.30	275.34	2730.75
3522.22	300.79	2808.78
4138.56	316.82	2856.05
4793.72	323.41	2872.14
5374.76	320.24	2857.06
5991.25	307.65	2810.79
6302.80	297.65	2775.62
6613.29	285.22	2732.67
7221.61	253.83	2625.48
7823.53	213.41	2488.91
8361.05	166.78	2199.42
8768.97	121.15	1732.70
9078.88	78.54	1188.05
9324.63	38.37	605.21

MODEL NAME DESADE

DRAG COEFFICIENT 1.55

CURRENT SPEED 7.5 CM/SEC

X-COORD (M)	Y-COORD (M)	Z-COORD (M)
204.63	72.11	599.27
452.64	149.38	1175.59
764.80	234.04	1712.53
1173.73	328.65	2169.86
1707.89	431.48	2450.66
2505.24	525.42	2582.41
2910.64	600.30	2686.16
3522.31	655.38	2761.02
4138.34	690.19	2806.31
4764.43	704.36	2821.61
5375.04	697.71	2806.80
5961.47	670.41	2761.96
6302.86	648.70	2727.89
6612.95	621.82	2686.41
7219.26	553.95	2583.02
7817.68	466.81	2451.57
8353.19	365.99	2170.86
8762.54	266.47	1713.56
9074.79	173.03	1176.53
9322.71	84.70	599.88

MODEL NAME DESADE

DRAG COEFFICIENT 1.55

CURRENT SPEED 10.0 CM/SEC

X-COORD (M)	Y-COORD (M)	Z-COORD (M)
210.24	122.89	589.06
464.61	253.98	1152.94
783.30	396.49	1673.94
1196.10	553.58	2110.79
1725.36	720.94	2372.30
2313.93	872.84	2492.26
2913.93	994.64	2586.92
3522.95	1084.67	2655.20
4138.31	1141.76	2696.37
4759.92	1165.07	2709.91
5376.17	1154.22	2695.64
5992.50	1109.51	2653.73
6303.66	1074.00	2622.04
6612.98	1030.02	2583.54
7215.00	919.48	2488.05
7806.03	778.33	2367.17
8337.03	614.14	2105.12
8749.22	449.28	1668.97
9066.38	292.62	1149.47
9318.96	143.49	587.32

INITIAL DISTRIBUTION LIST

Addressee	No. of Copies
ASN (RE&S)	1
OUSDR&E (Res. & Adv. Tech.)	1
ONR, ONR-100, -12, -222, -480, -486	5
CNO, OP-095, -098, -951, -951D, -951E, -951F, -952, -955, -981H	9
CNM, MAT 08L, -07, SPO PM-2 (2)	4
NAVELEXSYSCOM, PME-124 (3), ELEX 320 (3)	6
NAVSEASYSCOM, SEA-61R, -63R, PMS409A32 (F. Nystrom), PMS 409C (Dr. R. M. Snuggs), PMS409-517 (J. McGonegle)	5
NAVAIRDEVCEN	1
NOSC (R. Smith)	2
NAVWPNCEN	1
NAVPGSCOL	1
DTIC	10
DARPA (TTO)	4
NORDA (R. Swensen, R. Martin, R. Rumpf, R. Gardner)	4
SSPO (D. Viccione)	1
NRL (B. Adams)	2
NAVSURFWPNCEN, White Oak Laboratory	1
DWTNSRDC CARD	1
DWTNSRDC ANNA	1
CIVIL ENGINEERING LABORATORY, NAVAL CONSTRUCTION BATTALION CENTER, Port Hueneme, CA (D. Meggitt)	1